



375 276

# TECHNICAL NOTE

D-479

THERMAL-FATIGUE CRACK-GROWTH CHARACTERISTICS AND  
MECHANICAL STRAIN CYCLING BEHAVIOR OF A-286,  
DISCALOY, AND 16-25-6 AUSTENITIC STEELS

By Robert W. Smith and Gordon T. Smith

Lewis Research Center  
Cleveland, Ohio

NATIONAL AERONAUTICS AND SPACE ADMINISTRATION  
WASHINGTON

October 1960

...

(2)

...

THERMAL-FATIGUE CRACK-GROWTH CHARACTERISTICS AND MECHANICAL  
STRAIN CYCLING BEHAVIOR OF A-286, DISCALOY,  
AND 16-25-6 AUSTENITIC STEELS

By Robert W. Smith and Gordon T. Smith

SUMMARY

Thermal-fatigue crack-growth characteristics of notched- and unnotched-disk specimens of A-286, Discaloy, hot-cold worked 16-25-6, and overaged 16-25-6 were experimentally studied. Separately controlled variables were total strain range (0.0043 to 0.0079 in./in.), maximum cycle temperature (1300° and 1100° F), and hold time at maximum temperature (0 and 5 min). A limited number of mechanical, push-pull, constant-strain cycle tests at room temperature were made using notched and unnotched bars of the same materials. In these tests the number of cycles to failure as well as the variation of load change with accumulated cycles was measured, and the effects of mean stress were observed.

Constant-strain-range mechanical-fatigue tests at room temperature revealed notched-bar fatigue life to be strongly influenced by mean stress. For a specific strain range, the longest fatigue life was always found to be associated with the least-tensile (or most compressive) mean stress.

By defining thermal-fatigue life as the number of cycles required to produce a crack area of 6000 square mils, the relative thermal-fatigue resistances of the test materials were established. Notched-disk specimens of A-286 and Discaloy steels exhibited longer fatigue lives than either hot-cold worked or overaged 16-25-6. On the other hand, unnotched-disk specimens of Discaloy and hot-cold worked 16-25-6 had longer lives than A-286 and overaged 16-25-6. Separation of the crack-growth data into microstage and macrostage periods revealed that the macrostage period accounted for the greatest part of the difference among materials when tested in the notched configuration, while the microstage was largely responsible for the differences encountered in unnotched disks.

E-825

CY-1

## INTRODUCTION

The maximum cycle temperature of modern power-producing systems is increasing steadily, and many advanced propulsion schemes become attractive only when temperatures can be raised materially above current levels. Thermal-fatigue conditions, already a serious problem, will become more severe as working temperature limits are increased. Good design practices can reduce some physical constraints which give rise to thermal stresses. However, higher temperatures will tend to produce nonlinear thermal gradients, and unsteady operation of the high-power-concentration units of some nuclear systems can result in very severe transient temperature gradients.

The thermal stresses induced in a structural component depend on physical and mechanical properties of a material as well as on imposed design conditions. An attractive class of high-temperature materials, the austenitic steels, unfortunately has high coefficients of thermal expansion and low coefficients of thermal conductivity. Both of these characteristics tend to increase thermal stresses. Other mechanical characteristics of these materials favor their high-temperature applications, and specific data are therefore necessary for their evaluation under thermal-fatigue conditions.

Studies by Coffin (ref. 1) on AISI 347 austenitic stainless steel provided much information concerning the behavior of this material over a wide range of thermal strains. Clauss (refs. 2 and 3) has obtained similar information on S-816 (cobalt base) and Inconel 550 (nickel base) as well as the effect of thermal cycling on the subsequent stress-rupture life of the materials. The information available appears to indicate that, at temperature levels where metallurgical transformation effects are small, the number of cycles to failure is a simple function of the plastic strain imposed on each cycle. Manson (ref. 4) first suggested a relation between the number of cycles to failure and the cyclic plastic strain of the form

$$N_f = k/\epsilon_p^n \quad (1)$$

where  $k$  is a constant characteristic of the material. Constant-temperature mechanical strain cycling studies were performed on a series of materials (ref. 5), and the preceding equation fit the data well up to the strains of a simple tension test. A value of 2 for the exponent  $n$  was found to apply well in all cases. Clauss has demonstrated that the temperature level may cause a deviation from the simple plastic strain law when the maximum cycle temperatures are high enough to involve appreciable metallurgical transformation effects. Manson (ref. 6) has discussed these factors and the application of equation (1) to design situations.

E-825

Coffin and Clauss clamped the ends of their specimens and by alternately heating and cooling the test section introduced stresses that were uniform throughout the cross section where failure took place. In practice, however, thermal-fatigue damage usually does not appear in regions of uniform stresses but rather in regions of steep thermal-stress gradients. The damage in these cases is first indicated by the appearance of fatigue cracks (see e.g., ref. 7), which generally grow with continued cycling until either they move out of the high-thermal-stress region or fracture occurs because of superimposed loads acting upon the thermally fatigued region. The usefulness of equation (1) for stress-gradient thermal-fatigue problems characterized by the initiation and growth of fatigue cracks remains to be seen.

Reference 8 points out the importance of a phenomenological approach to fatigue problems by the study of fatigue-crack propagation. For this purpose the fatigue process is divided into two stages of crack propagation, microstage and macrostage. During the microstage progressive plastic deformation occurs in all grains where the local yield limit is exceeded. Annealed materials may strain-harden and hard materials strain-soften. Reversed slip then becomes concentrated in some regions within the grains, microcracks originate in these areas, and finally the microcracks grow and join together to form a macrocrack visible to the unaided eye. The macrostage involves the subsequent growth of these visible cracks usually leading to fracture.

1 CY-1 back

An experimental study was undertaken to evaluate the thermal-fatigue behavior of several alloys by measuring the growth of fatigue cracks during the cyclic process. Austenitic steels selected were A-286, Discalloy, and 16-25-6. Notched and unnotched disks  $3\frac{5}{8}$  inches in diameter by  $1/4$ -inch thick were rapidly heated to maximum cycle temperature  $T_{max}$  at the rim by induction, sometimes held at  $T_{max}$ , and then cooled to room temperature. Cycling produced cracks at the notch bottoms or at the rim of the unnotched disks. Growth of the cracks was followed by periodic microscopic measurements. Crack area as a function of number of cycles was plotted for each test. Notched disks were tested over a nominal strain range  $\epsilon_T$  of 0.0043 to 0.0079 inch per inch. Maximum cycle temperatures of  $1300^\circ$  and  $1100^\circ$  F were investigated. Unnotched disks were tested for a nominal strain range of approximately 0.0079 inch per inch at a maximum cycle temperature of  $1300^\circ$  F and for a strain range of 0.0066 inch per inch at a maximum cycle temperature of  $1100^\circ$  F. Tests incorporating a 5-minute hold time at  $T_{max}$  as well as no hold time were made for these conditions. The relative thermal-fatigue resistance of the various materials was evaluated by comparing the number of cycles to produce a specific crack size. In addition to the thermal-fatigue tests a few exploratory push-pull, mechanical-fatigue tests with

similar strain ranges were made on notched- and unnotched-bar specimens of these materials at room temperature. These tests permitted evaluation of the cyclic stresses and plastic strains which was not possible with the thermal-fatigue data.

Specific objectives of this investigation were the following:

- (1) To measure the progressive growth of thermal-fatigue cracks in both notched and unnotched disks for various conditions of  $T_{max}$ ,  $\epsilon_T$ , and hold time
- (2) To investigate in an exploratory manner the role of total stress range and mean stress upon constant-strain-range fatigue life of notched and unnotched bars at room temperature
- (3) To evaluate the relative thermal-fatigue resistance of A-286, Discaloy, hot-cold worked 16-25-6, and overaged 16-25-6 steels in both the notched- and unnotched-disk configuration
- (4) To study the effects of material and test variables upon the microstage and macrostage of crack growth.

## MATERIALS, APPARATUS, AND INSTRUMENTATION

### Materials Investigated

Three austenitic nickel-chromium steels, A-286, Discaloy, and 16-25-6, were investigated with 16-25-6 being studied both in a hot-cold worked and an overaged condition. Nominal compositions and heat treatments are indicated in table I. A-286 was heat-treated in billet form at the mill according to the manufacturer's recommended specifications for turbine wheel applications. Likewise, Discaloy and 16-25-6 were hot-cold worked according to manufacturer's recommended specifications for similar use. The overaging treatment given a separate lot of 16-25-6 produced a soft, relatively low-strength material for comparison with the other standard heat-treated steels. Tensile properties for notched and unnotched bars of these materials were measured at room temperature and 1300° F and are listed in table II. Tabulated values represent the average of two separate tests. These two tests were found to agree closely with one another in all cases.

### Specimen Configurations

Details of the thermal-fatigue specimen are shown in figure 1(a). The disks were nominally 0.250 inch thick and 3.595 inches in diameter.

Four equally spaced tool-cut notches were machined to the dimensions shown. A 0.166-inch hole at the center permitted the disks to be mounted on the drive shaft. Unnotched disks were investigated both as-ground and as-hand-polished with number 600 silicon-carbide paper.

Specimens (fig. 1(b)) used for the mechanical-fatigue program were machined from thermal-fatigue disk blanks and were, therefore, limited to a maximum thickness of 0.250 inch. Notches were made to the same specifications as used for the thermal-fatigue disks.

Specimens used for the tensile tests were similar to the mechanical-fatigue specimens (fig. 1(b)) except that the test-section length was 1 inch.

### Test Apparatus

Thermal fatigue. - A motor generator set was used to furnish induction heating to thermal-fatigue test rigs like the one shown in figure 2. The figure indicates that the cooling-air supply system serves also as the structural member of each rig. A pressure regulator was set to maintain a pressure of 0.1 pound per square inch upstream of bushings placed in the air distribution tubes directed into the center of both faces of the disk. This low-pressure cooling air flowed continuously throughout the heating, holding at  $T_{max}$ , and cooling portions of the thermal-fatigue cycle. To maintain uniform circumferential temperature distribution the disk was rotated at about 70 rpm by the illustrated drive mechanism. Thermocouple leads from the disk were passed through the hollow drive shaft to a slip-ring assembly.

Mechanical fatigue. - Room-temperature low-cycle mechanical-fatigue tests were carried out in the 20,000-pound direct push-pull fatigue machine shown in figure 3(a). The hydraulic load cylinder is attached to the base plate of the machine. Connected in series with the cylinder piston rod are a Baldwin load cell, the movable platen of a die set, and the lower specimen head. The upper specimen head is attached by means of split-cone, wedge-type grips (fig. 3(b)) to a short loading rod piloted and screwed into the upper die-set platen which is bolted to the upper frame of the machine. Attached to the lower movable platen is a 10:1 deflection lever that actuates microswitches for load reversal at preset deflection limits and causes automatic shutdown of the machine upon specimen fracture. The die set serves to maintain alignment, particularly under large plastic compressive strain. Accessory equipment not shown in the picture includes hydraulic pump and supply tank, accumulator, pressure regulator, solenoid valve, and other hydraulic accessories.

## Instrumentation and Control

Thermal fatigue. - Disk temperature was monitored continuously by recording the output of one Chromel-Alumel thermocouple bead 0.025 inch in diameter spotwelded into a small centerpunch mark on the disk rim. Ceramic high-temperature cement was painted over the spot-welded region. A rim thermocouple was used in all but the polished disk tests in which instances the thermocouple bead was spotted to the face of the disk 0.22 inch radially inward from the rim. This thermocouple position was first calibrated against a rim thermocouple on a special calibration disk providing an indirect means of monitoring rim temperature.

Timers were used to control the duration of each stage of the thermal-fatigue cycle and to operate solenoid switches or change alternator power settings through the use of suitable relays. The rate of induced heat generation within the disk was controlled by setting a potentiometer regulating field voltage in the alternator. One potentiometer was set to give the desired heating rate during the heating stage, and a second potentiometer was set at a lower value whenever a cycle included a hold period.

Mechanical fatigue. - Both total strain and load were measured during the room-temperature low-cycle mechanical-fatigue tests. Total strain range was measured with the usual arrangement of two 1-inch-gage-length Tuckerman optical strain gages clamped to opposite faces of the test specimen. Load was continuously recorded throughout the test by feeding the voltage output of a Baldwin load cell into a Leeds and Northrup recorder.

## PROCEDURE

### Thermal Fatigue

The general method of thermal-fatigue testing was to rapidly induction-heat the rim of the disk to a predetermined maximum temperature and then, by shutting off power, to cool back the rim at a relatively slow rate to room temperature. In some of the tests, the disk rim was held at  $T_{max}$  for 5 minutes following the rapid heat. Total strain range was controlled independently of temperature level by adjusting the heating rate of the induction coil.

Before routine thermal-fatigue testing was begun, it was necessary to calibrate the power supply and to determine the temperature distribution within the disk specimen for different heating rates and heating times. The temperature calibration was used, in turn, to compute total strain range at the disk rim, one of the independent test variables.

Calibration of power supply. - Prior to thermal-fatigue tests, the induction equipment was calibrated by determining the relation between power settings and times required to raise the rim temperatures to 1100° and 1300° F. Power levels for holding at maximum temperatures were also determined. Since only a two-step power system was available, the disk rim temperature dropped somewhat as the power level was switched from rapid heating to the "hold" level and then climbed back to  $T_{max}$  during the hold period.

Calibration of disk temperature and strain distribution. - Temperature distribution as a function of time was measured for each material by feeding the voltage output of seven radially spaced thermocouples into a multichannel oscillograph. Calibration temperature-time records were made for a series of heating rates to maximum cycle temperatures of 1300° and 1100° F. Figure 4 indicates typical temperature distribution against time for a 20-second heat up to 1300° F and hold at 1300° F. Selected temperature data of figure 4 were crossplotted to obtain figure 5(a), which shows the radial temperature distribution at the end of a 20-second heating period to 1300° F and at the end of the hold period at 1300° F.

Timoshenko and Goodier (ref. 9) present general thermal-stress equations for a symmetrical temperature distribution acting on thin disks from which the following equations can be derived by making use of the boundary conditions:

$$S_r(r_i) = S_r(r_o) = 0$$

$$\frac{S_\theta}{E\alpha} = \frac{r^2 + r_i^2}{r^2(r_o^2 - r_i^2)} \int_{r_i}^{r_o} T_r dr + \frac{1}{r^2} \int_{r_i}^r T_r dr - T \quad (2)$$

$$\frac{S_r}{E\alpha} = \frac{r^2 - r_i^2}{r^2(r_o^2 - r_i^2)} \int_{r_i}^{r_o} T_r dr - \frac{1}{r^2} \int_{r_i}^r T_r dr \quad (3)$$

These equations were solved with measured temperature distributions at the instant for which the stresses are desired by using a numerical finite difference procedure. Figure 5(b) shows the stress solution for these temperature profiles. The maximum stress occurs in the tangential direction at the disk rim except, in some instances (e.g., hold time at  $T_{max}$ ), for the local stress at the small center hole. The rim stress is compressive because of the restraint imposed by the relatively cool inner section. Similar calculations for other heating conditions revealed that the tangential rim stress increased compressively during the rapid heating portion of the fatigue cycle, reaching a maximum at the instant  $T_{max}$  was reached. When the temperature distribution is severe enough to

cause stresses in excess of the yield point, then, of course, the elastically computed stresses may be seriously in error. However, reference 10 shows for similar thermal-stress problems having steady-state thermal gradients that the elastically computed strain agrees well with the strain calculated from plastic theory. For this reason, the elastically computed disk rim tangential strain at the instant  $T_{\max}$  was reached,  $\epsilon_{o,\max}$ , was selected as the independent strain variable to be used in the experimental study. The mechanical strain is related to stress as follows:

$$\epsilon_o = \frac{S_{\theta,o}}{E} - \nu \frac{S_{r,o}}{E} = \frac{\beta_{\theta,o}}{E} \quad (4)$$

since  $S_{r,o} = 0$  at the rim. Disk rim strain  $\epsilon_{o,\max}$  was calculated by using equations (2) and (4) and assigning  $\alpha$  to be  $10^{-5}$  inch per inch per  $^{\circ}\text{F}$ , which is representative for all test materials. Since the materials used in this program have approximately the same values for  $\alpha$  and  $E$ , the nominal strain variable  $\epsilon_{o,\max}$  represents, essentially, a specific temperature distribution in the disk.

A few radial growth measurements verified a widely used thermal-fatigue assumption that the elastically computed strain  $\epsilon_{o,\max}$  was equal to the actual total strain range  $\epsilon_T$  (i.e., sum of elastic and plastic mechanical strain components) within the accuracy of the measurements. A dial indicator with a thermally insulated stem was set up to measure the radial expansion and contraction  $\Delta r$  of the disk rim during the thermal cycle. Tangential expansion per unit length equals  $\Delta r/r$  at the rim, and the total strain range can be calculated from the following equation:

$$\epsilon_T = \frac{\Delta r}{r} - \alpha \Delta T \quad (5)$$

where  $\Delta T = T_{\max}$  minus room temperature. Table III compares  $\epsilon_{o,\max}$  calculated from equation (4) with measured  $\epsilon_T$  showing that the difference between calculated and measured mechanical strain ranges does not exceed 3 percent of the elastically computed  $\epsilon_{o,\max}$ . For these reasons the independent thermal-fatigue strain range variable  $\epsilon_T$  has been set equal to  $\epsilon_{o,\max}$  as calculated from equation (4).

The following table lists the strain ranges and heating times to  $T_{\max}$  used in the experimental program:

$T_{\max}$ , °F	Heating time to $T_{\max}$ , sec	$\epsilon_T \equiv \epsilon_{O,\max}$ , in./in.	Disk configuration
1300	6.5	0.0079	Notched and unnotched
	10	.0074	Notched and unnotched
	20	.0066	Notched
	40	.0054	Notched
	80	.0043	Notched
1100	5	<sup>a</sup> 0.0066	Notched and unnotched
	21	.0054	Notched
	49	.0043	Notched

<sup>a</sup>Power supply did not have sufficient capacity to produce a greater strain range at 1100° F.

Two series of tests were run at the preceding conditions, one in which the specimen was immediately cooled upon reaching  $T_{\max}$ , and another in which the disk rim was maintained at  $T_{\max}$  for 5 minutes before cooling. Four or five minutes were allowed for cooling of the disks from  $T_{\max}$  to room temperature.

Method of crack measurement. - The initiation and growth of fatigue cracks was followed by viewing with a 20-power measuring microscope each of the notches or surveying the unnotched disk rim. After the crack started, the number of cycles between readings was selected to provide a reasonably uniform density of data points up to a crack area of at least 6000 square mils.

The initiation of cracks at a notch bottom was established by viewing the notch radially. After a continuous crack had formed across the notch bottom, the viewing microscope was directed at the disk faces and the length of crack along each face measured.

For smooth disks, the edges of the disk rim were scanned until cracks were located. Each crack was marked, and crack measurement records for several of the larger cracks were taken. Only the fastest growing crack has been indicated for each material in the subsequent presentation of unnotched-disk data.

The characteristic shapes of the fractured surfaces in notched and unnotched disks are shown in figure 6. Cracked areas were calculated from two measurements of crack length. For notched disks (fig. 6(a)), the product of one-half the sum of the measured crack lengths,

$\frac{1}{2}(l_1 + l_2)$ , times the disk thickness equaled the approximate crack

area. In the unnotched disks, cracks usually originated at or near the corner joining the face and rim of the disk (fig. 6(b)), producing an elliptical quadrant shape. The product  $\frac{\pi}{4} l_1 l_2$  gave the area. Figure 6(c) illustrates the appearance of fractured surfaces in unnotched disks which originated at the thermocouple spot weld. The large crack shown is nearly semicircular in shape, permitting a good estimation of area based on  $l_2$ .

### Mechanical Fatigue

Manual operation of the push-pull fatigue machine was necessary during the first few cycles of each test in order to set the deflection limit switches to produce the desired cyclic strain range  $\epsilon_T$  over the 1/2-inch test-section length. Since it was necessary to use Tuckerman gages having 1-inch gage lengths, the test-section strain was found by subtracting a quantity representing the elastic elongation of the 1/4-inch fillet and shoulder section at each end of the reduced test section (see appendix B). Each of the specimens was cycled between fixed strain limits, one limit in all cases being the initial test-section length of the specimen. The other limit corresponded to either an initial tensile strain of fixed amount (tension strain cycled) or an initial compressive strain of fixed amount (compression strain cycled). Once the initial strain  $\epsilon_T$  was realized, the nominal strain over the 1/2-inch test section was reduced to zero by applying a suitable load in the reverse direction. The load was then again reversed and the second cycle begun by loading in the initial direction to the desired strain  $\epsilon_T$ .

Automatic operation of the fatigue machine was begun once the limit switches had been positioned so that the deflection lever triggered the switches at the desired strain limits as observed with the Tuckerman gages. Usually three to six cycles were required to make these settings. Periodic checks were made of the nominal strain range  $\epsilon_T$  throughout the duration of the test. Whenever the load range changed significantly as a result of strain-hardening, strain-softening, or crack growth, it was necessary to make slight adjustments to the deflection lever micro-switch positions. Since these switches maintained constant deflection between upper and lower die heads, a decrease in load range, for example, increased the strain range at the test section because of the lowered elastic deflection of loading rods, grips, and specimen heads. Micro-switch adjustments were made whenever the strain range drifted 80 to 100 microinches per inch from the desired value.

Mechanical-fatigue tests were made for nominal strain ranges of 0.0075, 0.0070, and 0.0043 inch per inch over the 1/2-inch test section.

Periodic crack-growth measurements were not a part of the room-temperature fatigue program because Tuckerman extensometers clamped onto the specimen prevented viewing the sides of the test section with a microscope. However, when a test was stopped because of operational difficulties, crack size measurements were made by removing the specimens from the rig and examining them under a microscope.

## RESULTS AND DISCUSSION

### Thermal-Fatigue Crack-Growth Observations

Notched disks. - Figure 7 shows the basic data as plots of crack area against number of cycles for each notched Discaloy specimen, these being typical of all materials tested (total of 64 specimens). Each datum point of figure 7 represents the average of the four crack areas associated with the four machined notches equally spaced around the disk rim. Usually, the rate of crack growth increased with crack size until a fairly constant maximum growth rate was reached by the time the cracked area reached 6000 square mils. Exceptions were observed for Discaloy (fig. 7(c)) and A-286 notched disks tested at  $\epsilon_T = 0.0043$  inch per inch and  $T_{max} = 1100^\circ$  F. In these cases, the early crack growth rate followed the usual pattern of increasing with crack size, but a maximum growth rate was reached at about 2000 square mils with subsequent cycling producing a decreasing rate of crack growth. These data indicate that under certain thermal-fatigue conditions cracks initiating in notches subsequently may become nonpropagating just as is sometimes found in high-frequency fatigue testing (refs. 11 and 12).

Evidence of damage in the form of tiny irregular cracks or surface disruptions was often seen very early in the tests by viewing the notches radially. For the notched disks with no hold time, these first signs of failure varied from 3 to 23 cycles and were generally seen within the first 10 cycles. The growth and conjunction of these small cracks to produce an impression of a continual crack across a notch bottom usually required many times the cycles necessary to produce the first signs of damage. Much more cycling was often required before an indication of a growing crack was obtained by viewing the disk sides.

Photomicrographs (figs. 8, 9, and 10) show the as-heat-treated microstructure together with one or more views of thermal-fatigue-cracked areas for notched disks of each of the four test materials. Hot-cold worked 16-25-6 (figs. 10(a) and (b)) has a much smaller grain size than the other three materials. Overaged 16-25-6 (figs. 10(c) and (d)) exhibits the large amount of precipitates characteristic of this heat treatment. Except for the narrow band of recrystallization in the tool

cut worked region around the notch of the Discaloy specimen (fig. 9(b)), no appreciable changes to the microstructure were produced by thermal fatigue.

Figures 8(b), (c), and (d) show successive stages of crack growth in a notched A-286 disk cycled at a strain range equal to 0.0074 inch per inch between room temperature and 1300° F with a 5-minute hold time at  $T_{max}$ . Each photograph pictures a different notch, each notch region having been cut out of the disk after the specified number of cycles. Cracks in various notches penetrated to depths of approximately 0.0010, 0.0035, and 0.0054 inch after 5, 10, and 20 cycles, respectively. Residual tensile stresses pull the crack open at the cold portion of the thermal cycle, making detection and measurement easier. Compressive stresses at the hot portion of the cycle push the cracked surfaces together, causing a smoothing out of crack contours.

An examination of the crack tips reveals that crack propagation was sometimes transcrystalline and sometimes intercrystalline.

Microhardness measurements made for the region immediately ahead of a crack tip are shown in figure 11. Two hot-cold worked 16-25-6 disks having initial Vickers hardnesses of 294 and 289 softened to 253 and 246, respectively, at a distance 0.1 inch ahead of the crack front and to 253 and 248 at a distance of 0.01 inch. Two overaged 16-25-6 disks with original hardnesses of 193 and 180 hardened to 216 and 211, respectively, at 0.1 inch from crack front and to 246 and 227 at 0.01 inch. Cold-worked and annealed materials are likely to behave much more similarly during the macrostage of fatigue than expected from a comparison of virgin stress-strain relations, because these hardness measurements suggest that the flow properties of the two materials tend to become more alike in the region near the crack front.

Unnotched disks. - Cracks form at random locations around the periphery of unnotched disks. Somewhat more cycles are required to produce fine cracks in the unnotched disks than notched, yet these were seen before 20 percent of the number of cycles required to produce a 6000-square-mil crack. Early cracks in unnotched disks sometimes would develop at a fine scratch mark or at thermocouple spot welds, but usually the cracks appeared without apparent presence of surface defects. Generally, early cracks of unnotched disks remained very shallow in depth and almost dormant in growth for many cycles until finally a very measurable and increasing crack-growth rate was observed.

Only a few of the cracks reach appreciable sizes, the majority exhibiting comparatively slow growth rates. Usually the crack which eventually proves to be largest is seen when the first crack becomes visible with a low-power microscope; however, occasionally a later

appearing crack will grow very rapidly to become the largest one in the disk. Sometimes the macroscopic cracks may be near enough to one another so that further growth causes them to join together to form a single large crack. Unnotched Discalloy crack-growth data for a maximum cycle temperature of  $1300^{\circ}$  F are shown in figure 12. Each set of data points represents the fastest growing crack in that disk. Crack-growth rate increases with crack size, becoming large by the time the area is 6000 square mils.

#### Effect of Test Variables Upon Thermal-Fatigue Life

The effect of test variables upon thermal-fatigue life is indicated by the number of cycles required to produce a specific crack size. For design purposes, the limiting crack size should not be so small that useful life of the part is discarded, nor so big that danger of sudden failure exists; consequently, this size will depend somewhat upon design factors other than thermal fatigue. For the purpose of this thermal-fatigue investigation, the fatigue life is defined as the number of cycles required to produce a cracked area of 6000 square mils. In figure 13, nominal strain range  $\epsilon_T$  is plotted against number of cycles causing a 6000-square-mil crack  $N_{6000}$  in notched disks of A-286, Discalloy, hot-cold worked 16-25-6, and overaged 16-25-6. Fatigue life increases for all materials as  $\epsilon_T$  is decreased and as  $T_{max}$  is decreased from  $1300^{\circ}$  to  $1100^{\circ}$  F at constant  $\epsilon_T$ . A 5-minute hold time at  $T_{max}$  reduces fatigue life when  $\epsilon_T$  is large but has little or no effect at the lowest  $\epsilon_T$  of test.

Figure 13 also illustrates the relative notched-disk thermal-fatigue life of the various materials for specific conditions of  $T_{max}$  and hold time. Differences among materials are greatest at low values of strain range. The data for  $T_{max} = 1300^{\circ}$  F, with and without hold time at  $T_{max}$ , indicate that the materials rate in the following order of decreasing life: A-286, Discalloy, overaged 16-25-6, and hot-cold worked 16-25-6. For  $T_{max} = 1100^{\circ}$  F, the relative ratings of overaged 16-25-6 and hot-cold worked 16-25-6 interchange with one another without hold time. They also interchange at low strain ranges with hold time at  $T_{max} = 1100^{\circ}$  F.

Plots of crack-growth rate against nominal strain range (fig. 14) shed additional light on the thermal-fatigue behavior of these alloys. The growth rate was evaluated by measuring the tangents to the curves of crack area against  $N$  (such as fig. 7) at the 6000-square-mil point. Rate of crack propagation in notched disks increases with increasing  $\epsilon_T$  at constant  $T_{max}$  and with increasing  $T_{max}$  at constant  $\epsilon_T$ . Under

the same conditions of test, cracks propagate less rapidly in A-286 and Discaloy steels than in hot-cold worked and overaged 16-25-6 steels.

Relative material ratings in unnotched thermal fatigue can be evaluated by comparing the number of cycles  $N_{6000}$  required to produce a 6000-square-mil crack area (table IV). The differences among materials are not great, but a trend is indicated for ranking the alloys in the following order of decreasing merit: Discaloy, hot-cold worked 16-25-6, A-286, and overaged 16-25-6.

The comparison of unnotched thermal-fatigue life with notched disks is shown in table IV. Notches reduce the thermal-fatigue life to a small fraction ranging from 1/6 to 1/50 of the unnotched-disk life. The tabulated data also show hand-polished unnotched disks to have greater fatigue life usually than disks with the standard-ground surface finish.

#### Effect of Plastic Flow Upon Thermal-Fatigue Life

Although plastic flow was not an independent test variable, results of the present investigation agree with the concept that as  $\epsilon_p$  is increased  $N_f$  is reduced. The plastic flow per cycle  $\epsilon_p$  is related to total strain range per cycle  $\epsilon_T$ , the total stress range  $S_T$ , and the elastic modulus  $E$  by the following equation:

$$\epsilon_T = \frac{S_T}{E} + \epsilon_p \quad (6)$$

Since it was not possible to measure stress range during thermal-fatigue testing,  $\epsilon_p$  could not be quantitatively determined. Nevertheless, it is possible to show in a qualitative manner for a specific material that, whenever one thermal-fatigue test variable was changed in such a manner as to cause an increase in  $\epsilon_p$ , the life of the specimen was reduced. Test variables to be considered in this discussion are the effect of notches, total strain range, maximum cycle temperature, and hold time. Notched specimens failed in considerably fewer cycles than unnotched specimens when subjected to the same nominal strain range per cycle. The notch, of course, concentrates stress- and strain-producing localized plastic flow several times the amount of that in unnotched disks. Increasing the total strain range  $\epsilon_T$ , other variables being held constant, reduced fatigue life. Since plastic flow  $\epsilon_p$  increases (although nonlinearly) with increasing strain, again reduction of life is to be expected. Thermal-fatigue life was found to decrease when  $T_{max}$  was increased from 1100° to 1300° F,  $\epsilon_T$  being held constant. The yield strength of these materials decreases, thermal-expansion coefficient

increases, and the possibility of creep relaxation increases with this change in  $T_{max}$ ; consequently, an increase in the plastic component of  $\epsilon_T$  may be expected. Finally, the number of cycles to failure decreased or remained unchanged, depending upon strain range, when a 5-minute hold period at  $T_{max}$  was introduced into the cycle. Holding at  $T_{max}$ , if the stress is sufficiently high, permits additional plastic flow in the form of creep to occur during each cycle. All decreases in life for a specific material cited previously are associated with changes in test variables which are expected to increase the plastic flow per cycle.

#### Microstages and Macrostages of Crack Growth

Since thermal-fatigue crack-growth data will be used to study the relative influence of test and material variables upon the two stages of the fatigue process, it is necessary to separate the total fatigue life (cycles required to produce a cracked area of 6000 sq mils) into periods of microstage and macrostage of crack growth. The choice of crack size separating these two stages is not critical so long as the intent of the description of reference 8 is kept in mind. For the purpose of this analysis, a crack area of 500 square mils was selected to separate the two stages of fatigue. Such a crack in the notched-disk specimen has a radial depth of 2 mils and is readily seen by looking down into an illuminated notch bottom. A somewhat smaller area might have been chosen if it were not for the increasing inaccuracy in crack area measurements as crack size becomes smaller. The microstage duration is defined, therefore, as the number of cycles required to produce a crack area of 500 square mils,  $N_{500}$ , and the macrostage duration as the number of cycles required to enlarge a crack from 500 to 6000 mils,  $500N_{6000}$ . The length of each of these stages for notched disks is plotted in figure 15 against nominal strain range for  $T_{max} = 1300^\circ \text{ F}$  and  $1100^\circ \text{ F}$ , with and without 5-minute hold periods at  $T_{max}$ .

Comparison of the two fatigue stages (figs. 15(a), (c), (e), and (g) with 14(b), (d), (f), and (h), respectively) reveals the microstage to be shorter and much more similar for the various materials than the macrostage period. Apparently, the stress and strain concentration caused by the notch far overshadows microstructural or mechanical material properties which may otherwise significantly affect crack initiation. The observed differences between materials in notched-disk thermal-fatigue life result primarily from the macrostage of the fatigue process. On the other hand, the microstage period generally represents the major portion of unnotched-disk thermal-fatigue life (table IV), and it is this stage of the process which accounts for the major portion of the differences in unnotched fatigue lives among the various alloys.

## Mechanical Low-Cycle Fatigue Tests

Constant-strain-range, push-pull, low-cycle fatigue testing at room temperature provided data on the number of cycles causing fracture (complete separation of the test section) together with the variation of maximum tensile and compressive loads with  $N$ . Figure 16 schematically illustrates the hysteresis loops developed in low-cycle fatigue tests and indicates the cycle variables of  $\epsilon_T$ ,  $\epsilon_P$ ,  $S_T$ , and  $S_M$ . The test information was used to make plots of total stress range and mean stress as a function of  $N$  such as shown for unnotched and notched Discaloy specimens in figures 17(a) and (b), respectively. These data, which are quite typical of the mechanical low-cycle fatigue results, show the total stress range to increase slightly, in some cases, at the beginning of test, hold fairly constant for a period, and then decrease at a gradually increasing rate as macroscopic crack growth accelerates. Mean stress remains fairly constant during the first part of the test and then falls off to higher compressive values during the latter part of the test because of the loss of the tension-carrying ability of the material as the crack enlarges. The dashed horizontal lines define an arbitrary stress range equal to either 5 or 10 percent of the total stress range at  $N = \frac{1}{2} N_F$ . The 10-percent range is applied to the total stress range and the 5 percent to the mean stress, with the upper limit of the range in each case passing through the highest tensile datum point. The purpose of these lines is to give an indication of the duration  $N_{S_T}$  and  $N_{S_M}$ , in terms of percent of  $N_F$ , of the periods in which total stress range and mean stress, respectively, remain within these fairly narrow limits. It is seen for the unnotched Discaloy bar (fig. 17(a)) that the total stress range remains in this region for about 78 percent of  $N_F$  and the mean stress 77 percent of  $N_F$ . For the notched Discaloy bar (fig. 17(b)) the percentages are 50 and 88, respectively. Similar data for all the mechanical-fatigue tests (table V) showed that total stress range remained within these narrow limits for 50 to 100 percent of the total life and the mean stress for 52 to 99 percent  $N_F$ . Since the total stress range  $S_T$  and the mean stress range  $S_M$  at  $N = \frac{1}{2} N_F$  are representative values for at least one-half the total specimen life, it seems justifiable to use these parameters for subsequent analyses of test results.

Table V also lists for each mechanical-fatigue test the magnitude and direction of applied strain range  $\epsilon_T$ , number of cycles to failure  $N_F$ , mean stress  $S_M$  at  $\frac{1}{2} N_F$ , and total stress range  $S_T$  at  $\frac{1}{2} N_F$  for both notched and unnotched specimens. Perhaps the most interesting fact revealed by these exploratory tests is the large effect that direction of applied strain range has upon notched-bar fatigue life

at an applied strain range of 0.0043 inch per inch (table V(a)). Compression-strain-cycled specimens of A-286, Discaloy, and hot-cold worked 16-25-6 exhibited lives ranging from 9 to 70 times that for tension-strain-cycled specimens. On the other hand, overaged 16-25-6 showed little effect due to direction of applied strain under the same imposed strain range. Hot-cold worked 16-25-6 demonstrated the longest life of the four materials when compression strain cycled and the shortest life when tension strain cycled. These effects are associated with mean-stress level, which is to be discussed subsequently. The relative ratings of the four materials (table V) vary with changes in strain cycling direction, in specimen configuration (i.e., notched or unnotched), and in the applied strain range.

Effect of mean stress. - The effect of mean stress upon notched-bar mechanical-fatigue life is readily illustrated by figure 18. Here total stress range and mean stress at  $\frac{1}{2} N_f$  are plotted against logarithm of fatigue life for notched specimens subjected to a nominal total strain range over a 1/2-inch test section of 0.0043 inch per inch. Total stress ranges for three of the materials, A-286, Discaloy, and hot-cold worked 16-25-6, happen to be approximately equal regardless of initial strain cycling direction. Mean stress for these materials is seen to depend both upon material and direction of strain cycling. Compression strain cycling (compressive initial loading) produced compressive mean stresses, and tension strain cycling (tensile initial loading) produced tensile mean stresses. The relative fatigue-life ranking of the three materials having approximately equal total stress ranges was directly related to the relative values of mean stress developed, the algebraically lowest mean stress corresponding to the longest life. According to the line passed through the data points, a tenfold decrease in life results from a 52-ksi increase in mean stress.

Mean-stress data for overaged 16-25-6 fall to the left, and total stress falls below the data for the other materials. If one were to insert the total stress and total strain range information into equation (6), the calculated nominal plastic flow for overaged 16-25-6 would be substantially greater than that for the other materials. It is believed that this larger nominal plastic flow per cycle causes the mean-stress data of overaged 16-25-6 to fall to the left of the other materials. Although the experimental range of mean stress was not large for overaged 16-25-6, the data indicate a trend of increasing life with algebraically decreasing values of mean stress similar to the other materials.

Nominal mean stress for a given set of constant-strain-cycling conditions is dependent upon the cyclic stress-strain behavior of the material. So long as the specimen is cycled between its original length and some predetermined value of strain, the maximum possible magnitude

of the mean stress will be one-half the total stress range. This takes place when the nominal stress cycles between zero and the yield point (for the particular stress state) of the material. If the applied strain range is increased causing the maximum nominal stress to exceed the yield point, the magnitude of the mean stress will decrease, approaching zero at sufficiently large values of applied strain range for materials having the same flow properties in tension as compression. Hot-cold worked 16-25-6 initially loaded in compression to 0.0043 inch per inch had a mean stress of -51.7 ksi equal to 83 percent of one-half  $S_T$ . Hence, the strain range of 0.0043 inch per inch is near the condition producing maximum mean-stress level effect for notched bars of this material. On the other hand, at this same strain range specimens of overaged 16-25-6 with mean stresses no more than 16 percent of one-half  $S_T$  are strained well beyond the region of maximum mean-stress level effect, and for this reason the direction of initial loading has little effect upon life.

It is interesting to note that notched overaged 16-25-6 bars have a greater life than any of the other materials for tension strain cycling at  $\epsilon_T = 0.0043$  inch per inch despite the fact that nominal  $\epsilon_p$  is greater than the others. Apparently, the relatively low tensile value of mean stress causes a beneficial effect greater than the detrimental effect of nominal  $\epsilon_p$  in this case. Figure 13 shows that, for a given  $\epsilon_T$ , overaged 16-25-6 is inferior to the other materials when compared for the same value of mean stress but is superior when compared for the case of tension strain cycling.

Unnotched bars, like notched bars, developed shorter lives when tension cycled than compression cycled. The observed effect upon life was not as great as found for the notched bars because the selected strain range of test did not produce magnitudes of mean stresses which were a large percentage of one-half the total stress range. Also, the effect is less important with unnotched than notched bars for reasons associated with a crack-growth behavior which will be described subsequently. Table V(b) shows the tension-strain-cycled lives of A-286, Discaloy, and hot-cold worked 16-25-6 to be about 50 percent of the compression-strain-cycled lives for a nominal strain range of 0.0070 inch per inch.

The nominal plastic flow  $\epsilon_p$  was slightly greater for tension-strain-cycled bars than compression-strain-cycled bars, and for this reason some reduction of life would be expected. Consequently, the relative contribution of increased mean stress and increased plastic flow toward reduced life cannot be clearly evaluated with the limited amount of data. Overaged 16-25-6 again shows little effect of loading direction upon life since both mean stress and total stress range are practically unchanged at this level of strain range.

Crack-growth measurements. - Crack-size measurements were made during mechanical-fatigue tests only for three instances where notched specimens were removed from the rig before failure. These limited data (table VI) indicate (1) that large cracks can exist very early in the fatigue process as evidenced by a cracked area equal to 17 percent of the original cross-sectional area at 20 percent of total life, (2) that the number of cycles (about 39,000 compared with about 56,000) required to produce a macroscopic crack of about one-third the original cross-sectional area in notched specimens is more similar for the two materials than the number of cycles (about 12,000 and 137,000) required to continue the propagation of this crack to fracture, and (3) that the observed difference in fatigue life for these two materials arises most likely from the difference in mean stress because nominal strain range and total stress range are the same.

#### Comparison of Calculated Fatigue Life with Test Data

Design situations involving either thermal or mechanical fatigue require an estimation of useful life without the necessity of running an elaborate test program. It should be interesting, therefore, to examine how well equation (1),  $N_f = k/\epsilon_p^n$ , predicts the test results reported herein.

Since failure by thermal or mechanical fatigue in general involves both a microstage and a macrostage period, the reliability of the results obtained from equation (1) may differ depending on which period is dominant. The experimental data correlated with this equation by Coffin and others apply to situations in which the microstage period represented the major part of the life since direct push-pull tests with unnotched specimens were used to establish these relations. In these tests, the entire cross section was uniformly loaded and deterioration of all elements probably advanced relatively uniformly until all were close to failure. Coffin and Tavernelli (ref. 13) attempted to eliminate the crack-propagation period (macrostage) from the data correlation of unnotched specimens. Their success in correlating a wide range of materials with a relation of the form of equation (1) attests to the correctness of confining the relation to the microstage period. For this reason, this equation might be expected to predict a thermal-fatigue life which falls within or close to the microstage period. When used to predict the mechanical-fatigue specimen life, the equation would be expected to predict the measured fatigue life of the unnotched specimens but only the initial cracking of the notch bottoms for the notched tests. Because no data on initial cracking of the notched specimens were obtained, this comparison could not be made.

E-825

CY-3 back

Predicted lives for both the thermal- and mechanical-fatigue tests were calculated using tensile ductilities as suggested by Tavernelli and Coffin (ref. 5). The constant  $k$  in equation (1) was evaluated by assuming an exponent  $n$  of 2 and the tensile ductility,  $\ln(A_I/A_F)$ , as representing the cyclic plastic flow for  $N = 1/4$  cycle. Thus,

$$N_F \epsilon_p^2 = \frac{1}{4} \left[ \ln \left( \frac{A_I}{A_F} \right) \right]^2 = k \quad (7)$$

The unnotched tensile ductilities at both room temperature and 1300° F were used to establish the values of  $k$  used for the thermal-fatigue calculations.

Evaluation of the cyclic plastic flow  $\epsilon_p$  for the thermal-fatigue specimens was obtained by applying a strain concentration factor  $C$  to the total strain range in equation (6). For the notched-disk calculations,  $C$  was taken as 4.3, the value in reference 14 for a notch of this configuration, and as 1 for the unnotched specimens. No load measurement data were available for thermal-fatigue tests, and the plastic flow was calculated from the 0.2-percent-yield-point tensile data as follows:

$$\epsilon_p = C \epsilon_T - \left( \frac{S_{y,max}}{E_{max}} + \frac{S_{y,min}}{E_{min}} \right) \quad (8)$$

where  $S_{y,max}$  and  $E_{max}$  were evaluated at  $T_{max}$ , while  $S_{y,min}$  and  $E_{min}$  were evaluated at room temperature. The values of  $S_y$  were determined from the tensile data (table II), and the values for the elastic modulus were taken from the literature.

For the mechanical-fatigue data,  $\epsilon_p$  was evaluated in two different ways. The first method, similar to that employed for the thermal-fatigue tests, required only tensile data and would be readily available to a designer:

$$\epsilon_p = \epsilon_T - \frac{2S_y}{E} \quad (9)$$

The second and most accurate method made use of the measured load data:

$$\epsilon_p = \epsilon_T - \frac{S_T}{E} \quad (10)$$

Thus, two values of predicted life were obtained for thermal-fatigue data (based upon tensile ductilities at room temperature and 1300° F, respectively) and two values of predicted life for the

mechanical-fatigue data (based upon measured yield stresses and measured stress ranges, respectively). Table VII presents the thermal-fatigue notched-disk results and table VIII the unnotched mechanical-fatigue results.

Table VII lists the predicted lives as determined from equation (7), and the actual crack areas existing at the predicted time of failure. Predicted life for most cases fell within the microstage period for Discaloy, A-286, and overaged 16-25-6 when based on the tensile test showing the least ductility. The hot-cold worked 16-25-6 steel was an exception at both 1300° and 1100° F temperature levels. The high ductility exhibited by hot-cold worked 16-25-6 in the tensile tests was not accompanied by the capacity for absorbing plastic strain as predicted by equation (7). This material appears to be unusually susceptible to rapid thermal-fatigue crack growth in the presence of notches.

No unnotched-disk comparisons are shown because, with the exception of overaged 16-25-6, plastic strains near zero and a consequent prediction of an infinite or very long life were obtained. As will be subsequently illustrated for the mechanical-fatigue data, use of equation (1) for low strain ranges in conjunction with only tensile data will produce unsatisfactory results.

Table VIII can be used to further illustrate the point noted in connection with the unnotched disks. The ratio of predicted life based on twice the room-temperature yield strength and the actual life for A-286, Discaloy, and hot-cold worked 16-25-6 shows large overestimation of life. Hot-cold worked 16-25-6 calculations, like those for the unnotched disks, gave a zero value of  $\epsilon_p$  and an infinite life. Since the total strain range of the mechanical-fatigue specimens was carefully controlled, the poor predicted results are due principally to the use of yield strength data in equation (9). If strain-softening occurs, as is often the case with hardened materials (ref. 13), the elastic strain estimated from the tensile yield data will be larger than the specimen experiences and the plastic strain will be underestimated. The result will be a predicted life in excess of the actual life. Also, reference 13 indicates that, in general, the larger the applied strain range, the greater is the tendency toward strain-hardening. This is true even for materials with a considerable amount of previous work-hardening. As a result, the magnitude of the strain range as well as the prior strain history will influence the actual plastic-strain range. Estimates of cyclic plastic flow based on tensile yield strengths may, then, deviate very considerably from the actual plastic strain. In general, when the total strain range is in the neighborhood of twice the yield point, the tendency toward strain-softening will be the greatest and the chance of underestimating the plastic strain will be largest.

Also, because of the small values of plastic strain at this condition, the percentage error in plastic flow may be very large.

Figure 19 indicates how a relative error in life  $\Delta N/N$  is related to a relative error in plastic strain  $\Delta \epsilon_p/\epsilon_p$  for a material following the failure law of equation (7). It is apparent that underestimation of the plastic strain of 50 percent or greater will produce dangerously nonconservative predictions of life, whereas overestimation will result in conservative and smaller errors.

Comparison of the calculated lives (table VIII) based on measured stress ranges, using equation (7), with the actual lives will test the degree to which the tensile ductility and the exponent 2 reflect the fatigue characteristics. For A-286, Discaloy, and hot-cold worked 16-25-6, the ratio of predicted to actual life indicates that the tensile ductility can be used with reasonable accuracy to predict the fatigue life. Predicted lives are generally within a range of one-half to twice the actual lives and, in view of the scatter generally associated with fatigue data, should represent useful engineering estimates. For overaged 16-25-6, the tensile ductility and the exponent 2 did not permit a satisfactory prediction of the fatigue performance. As a result, predictions based on values of  $k$  established from a tensile test alone can be misleading, and data obtained from one or more constant-strain fatigue tests may be necessary where a high degree of reliability is required.

#### RELATION OF FATIGUE FACTORS TO CRACK PROPAGATION

It is believed that an understanding of the low-cycle fatigue behavior of materials subjected to steep stress gradients such as those produced by temperature gradients and/or notches can best be gained by studying the effect of the factors found to be important upon the initiation and growth phases of fatigue crack propagation. For this analysis, the fatigue process was divided into two stages of crack development, microstage and macrostage, as suggested in reference 8. During the microstage, cracks initiate within individual crystals, traverse across grain boundaries to join together with adjacent crystalline cracks, and finally enlarge to the point where they become visible to the unaided eye. During the macrostage, the cracks usually continue to enlarge, causing eventual loss of structural usefulness. The reason for separating the fatigue process into stages is that each stage may be differently affected by the various factors bearing upon fatigue life. With an understanding of the relative influence of the important fatigue factors upon the two stages of fatigue, and with experimental evidence regarding the duration of the two stages, it may be possible to determine specific reasons for the observed behavior of materials in fatigue.

Results of the present investigation, together with data discussed in reference 8, demonstrate that the microstage period makes up the greatest part of the total fatigue life for unnotched specimens, whereas the macrostage represents the greatest part of the notched-specimen fatigue life. Materials rating in one order when tested in the notched configuration should not necessarily rate in the same order when tested in the unnotched configuration.

#### Microstage

Factors believed to have an important influence upon the microstage duration of low-cycle fatigue are the following:

- (1) Amount of plastic flow per cycle
- (2) Material tolerance to accumulated plastic flow
- (3) Surface imperfections and/or microstructural discontinuities
- (4) Residual stresses
- (5) Grain size
- (6) Stress corrosion.

Other things being equal, increasing the amount of plastic flow per cycle represents an increase of the energy input into the crystal-line structure. Part of this increased energy will go toward the destruction of atomic bonds; hence, any increase in energy input per cycle will shorten the microstage period of the fatigue process. Low-cycle fatigue life has been successfully correlated with cyclic plastic flow by equation (1) for tests in which microstage duration comprises practically the entire specimen life. These correlations depend upon an accurate determination of  $\epsilon_p$ , such as obtained from measured total strain and total stress ranges.

Coffin suggests (ref. 1) that the tolerance to total accumulated plastic flow is directly related to tensile ductility when expressed by the parameter  $\ln(A_I/A_F)$ , where  $A_I$  is the initial cross-sectional area and  $A_F$  is the final area after fracture in a tensile test. These values are listed in table II for smooth-bar tensile tests at room temperature and 1300° F. Tensile ductility for a specific material as well as the relative ductilities of several materials may change with temperature so that an evaluation of the ductility effect in thermal fatigue is complicated by the fact that compressive plastic flow occurs at temperatures near  $T_{max}$  and tensile plastic flow at intermediate or

low-cycle temperatures. For notched specimens any effect due to the slight differences in ductility among the materials of test seems to be far overshadowed by mean-stress or plastic strain range variables in mechanical-fatigue tests at room temperature.

Surface imperfections and discontinuities in the microstructure are likely to act as local stress raisers, increasing the possibility of microscopic crack initiation at these places. Those disk specimens which were carefully hand-polished (table IV) generally developed longer fatigue lives than the unpolished disks. A-286 alloy was susceptible at times to failure originating beneath the surface, thus pointing to the likelihood of internal flaws.

Residual stresses may or may not have significant effect upon the microstage duration, depending upon the magnitude of the applied strain range. If the strain range is large enough to produce a stress range greater than twice the yield point, then the initial residual stresses are likely to be eliminated very quickly by strain cycling. At lower values of strain range, residual stresses may accelerate or decelerate crack initiation, depending upon whether they add or subtract from the major applied stress. Discaloy and hot-cold worked 16-25-6 unnotched disks were both susceptible to failure originating at the point where the thermocouple bead was spotwelded to the disk rim. Apparently, this region of steep residual stress gradients was less resistant to crack formation than other undisturbed points along the disk rim.

Small grain size should be beneficial since the grain boundaries act as barriers against the extension of small transcrystalline cracks. The relatively good showing of hot-cold worked 16-25-6 in the unnotched configuration may be partially attributed to its small grain size.

Finally, the high stresses associated with strain cycling will accelerate the damaging effects of corrosion and shorten fatigue life in the presence of corrosive atmospheres.

#### Macrostage

Factors believed to have a direct influence upon the macrostage duration are the following:

- (1) The distribution of plastic flow per cycle in the region into which the crack is moving
- (2) Material tolerance to accumulated plastic flow
- (3) The nominal mean stress.

E-825  
CY-4

The distribution of plastic flow in advance of the crack front depends upon the nominal stress, geometry of the notch and/or crack, and the stress-strain characteristics of the materials. Under the same test conditions, the stress-strain characteristics of the material will then control the distribution of plastic flow. In general, for a constant-strain amplitude, the material with the smallest stress range will undergo the most plastic flow at the crack front and have the largest area of plastic flow in advance of the crack. Initially soft materials may strain-harden and initially work-hardened materials soften, so that the stress-strain properties near the crack front may be much more alike than those of the original test specimens. Plastic-flow distribution at the beginning of the macrostage is quite different in the unnotched disk as compared to the notched. The strain-concentrating effects of the small crack alone are not as great as they are for the combination notch and crack. Usually unnotched-disk cracks originate near the corner, spreading radially inward and transversely across the thickness of the disk. The length of the crack front increases with cycles but is usually shorter than notched-disk crack fronts throughout the entire macrostage period  $500^N 6000$ . As a result, the macrostage period is longer in absolute duration in unnotched disks than notched, although a lesser percent of total life.

Nominal mean stress was apparently an important factor controlling fatigue life of notched bars undergoing mechanical fatigue. It is believed that mean stress has a much larger effect upon the macrostage than the microstage because strain concentration at the crack front is directly influenced by the direction of the applied nominal stress. Since tensile forces cannot be carried across a crack surface, tensile stresses are concentrated about the leading edge of the crack. Compression forces, on the other hand, will close the crack faces together, permitting some or all of the compressive load to be transferred across the broken surface, resulting in a lesser concentration of compressive stresses at the crack front. For this reason, local plastic flow per cycle will be greater in specimens with more tensile mean stress when subjected to the same nominal strain change per cycle and about the same total stress change. Considered from this viewpoint, mean stress is not another independent fatigue factor separate from plastic flow, but simply a variable which alters localized plastic flow.

#### CONCLUSIONS

Thermal crack-growth characteristics and mechanical constant-strain fracture data were obtained with four austenitic materials. Principal results were the following:

1. Low-cycle fatigue life (thermally cycled or mechanically cycled at constant temperature) of a specific material decreased whenever the plastic flow per cycle was increased.

2. Room-temperature, constant-nominal-strain-range, mechanical-fatigue testing of notched bars indicated fatigue life to be strongly influenced by mean stress (a variable dependent upon the stress-strain properties of the material and strain range of test). For materials developing about the same total stress change at  $\frac{1}{2} N_f$ , longer fatigue life is associated with the alloy having the least tensile (or most compressive) mean stress at  $\frac{1}{2} N_f$ .

3. A-286 and Discaloy exhibited better notched-disk thermal-fatigue resistance than hot-cold worked or overaged 16-25-6 although this difference was large only at the lowest values of maximum cycle temperature (1100° F) and strain range (0.0043 in./in.) of test.

4. Discaloy and hot-cold worked 16-25-6 generally demonstrated better thermal-fatigue resistance than A-286 and overaged 16-25-6 when tested in the unnotched configuration.

5. The macrostage period accounts for the greatest part of the differences between materials in notched-disk thermal-fatigue life.

6. The relative ratings of materials in unnotched-disk thermal fatigue largely depend upon factors which influence the microstage of the fatigue process.

Lewis Research Center  
National Aeronautics and Space Administration  
Cleveland, Ohio, July 28, 1960

## APPENDIX A

## SYMBOLS

A	area, sq mils
a	constant
C	strain-concentration coefficient
E	elastic modulus, lb/sq in.
e	elongation, in.
k	material constant
L	length, in.
l	crack dimension, mils
N	cycles
n	material constant
P	load, lb
r	radius, in.
S	stress, lb/sq in. or ksi
T	temperature, °F
$\alpha$	thermal-expansion coefficient, in./in.-°F
$\epsilon$	strain, in./in.
$\nu$	Poisson's ratio

## Subscripts:

e	elastic
f	fracture, or at 6000 sq mils
I	initial
i	inner

E-825

CY-4 back

M	mean
m	measured
max	at maximum cycle temperature
min	at minimum cycle temperature
o	outer
p	plastic
p,max	predicted based on 1300° F tensile data
p,min	predicted based on room-temperature tensile data
p,1	predicted based on measured stress range
p,2	predicted based on room-temperature tensile yield data
r	radial
T	total
y	0.2-percent yield
$\theta$	tangential
500	at 500-sq-mil crack area
6000	at 6000-sq-mil crack area

## APPENDIX B

## STRAIN RANGE CALCULATION FOR MECHANICAL-FATIGUE TESTS

For the mechanical, low-cycle fatigue tests, the total strain  $\epsilon_T$  was determined from measurements made with 1-inch-gage-length Tuckerman extensometers. Since the specimen test-section length was 1/2 inch, the axial deflections in the specimen shoulder and fillet sections were computed and subtracted from the measured elongation  $e_m$ . The remaining elongation was assumed to take place uniformly over the test section and was converted to nominal total strain by dividing by the test-section length.

The deflections of the shoulder and fillet regions were assumed to be elastic and are given by the following equations:

$$e_{\text{shoulder}} = \left(\frac{P}{E}\right)\left(\frac{L}{A}\right)_{\text{shoulder}} = a_{\text{shoulder}}P$$

$$e_{\text{fillet}} = \left(\frac{P}{E}\right)\left(\frac{L}{A}\right)_{\text{fillet}} = a_{\text{fillet}}P$$

where

$L$  = total length

$$a_{\text{shoulder}} = \frac{1}{E}\left(\frac{L}{A}\right)_{\text{shoulder}}$$

$$a_{\text{fillet}} = \frac{1}{E}\left(\frac{L}{A}\right)_{\text{fillet}}$$

The area of the fillet section was taken as the average of the areas of the test-section and shoulder regions. The test-section nominal strain was then

$$\epsilon_T = \frac{e_m - (a_{\text{shoulder}} + a_{\text{fillet}})P}{L_{\text{test section}}} = 2e_m - aP$$

where

$L = 1/2$  in.

$$a = 2(a_{\text{shoulder}} + a_{\text{fillet}})$$

## REFERENCES

1. Coffin, L. F., Jr.: Design Aspects of High-Temperature Fatigue with Particular Reference to Thermal Stresses. Trans. ASME, vol. 78, no. 3, Apr. 1956, pp. 527-532.
2. Clauss, Francis J., and Freeman, James W.: Thermal Fatigue of Ductile Metals. I - Effect of Variations in the Temperature Cycle on the Thermal-Fatigue Life of S-816 and Inconel 550. NACA TN 4160, 1958.
3. Clauss, Francis J., and Freeman, James W.: Thermal Fatigue of Ductile Metals. II - Effect of Cyclic Thermal Stressing on the Stress-Rupture Life and Ductility of S-816 and Inconel 550. NACA TN 4165, 1958.
4. Manson, S. S.: Behavior of Materials Under Conditions of Thermal Stress. Symposium on Heat Transfer, Eng. Res. Inst., Univ. Mich., 1953, pp. 9-76. (See also NACA Rep. 1170, 1954. (Supersedes NACA TN 2933.))
5. Tavernelli, J. F., and Coffin, L. F., Jr.: A Compilation and Interpretation of Cyclic Strain Fatigue Tests on Metals. Trans. Am. Soc. Metals, vol. 51, 1959, pp. 438-450; discussion, pp. 450-453.
6. Manson, S. S.: Thermal Stresses in Design. Machine Design, pt. 3, vol. 30, no. 16, Aug. 7, 1958, pp. 100-107; pt. 4 - vol. 30, no. 17, Aug. 21, 1958, pp. 110-113; pt. 5 - vol. 30, no. 18, Sept. 4, 1958, pp. 126-133.
7. Johnston, James R., Weeton, John W., and Signorelli, Robert A.: Engine Operating Conditions that Cause Thermal-Fatigue Cracks in Turbojet-Engine Buckets. NASA MEMO 4-7-59E, 1959.
8. Schijve, J.: Fatigue Crack Propagation in Light Alloys. M.2010, Nat. Aero. Res. Inst. (Netherlands), July 1956.
9. Timoshenko, S., and Goodier, J. N.: Theory of Elasticity. Second ed., McGraw-Hill Book Co., Inc., 1951, p. 407.
10. Mendelson, A., and Manson, S. S.: Practical Solution of Plastic Deformation Problems in the Elastic-Plastic Range. NASA TR R-28, 1959. (Supersedes NACA TN 4088.)
11. Fenner, A. J., Owen, N. B., and Phillips, O. E.: The Fatigue Crack as a Stress Raiser. Engineering, vol. 171, no. 1, May 1951, p. 637.
12. Frost, N. E., and Dugdale, D. S.: The Propagation of Fatigue Cracks in Sheet Specimens. Jour. Mech. Phys. of Solids, vol. 6, no. 2, 1958, pp. 92-100.

13. Coffin, L. F., Jr., and Tavernelli, J.: The Cyclic Straining and Fatigue of Metals. Rep. 58-RL-2100, General Electric Res. Lab., Oct. 1958.
14. Neuber, H.: Theory of Notch Stresses: Principles for Exact Stress Calculation. Trans. 74, David Taylor Model Basin, Nov. 1945.

TABLE I. - MATERIAL DESCRIPTION

Material	Composition	Condition	Finish hardness
A-286	C 0.05, Fe 53.3, Cr 15, Ti 1.6, Ni 26, Al 0.17, Mo 1.15, V 9.2, Mn 1.4	1650° F; 2 hr oil quench; age 1325° F, 16 hr; air-cooled	Rockwell C-26 to C-31
Discaloy	C 0.05, Fe 54, Cr 13, Ti 1.6, Ni 26, Al 3, Mo 3	89-Percent reduction; start at 1930° F, finish at 1475° F	Rockwell C-25 to C-30
Hot-cold worked 16-25-6	C 0.09, Fe 50.5, Cr 16, N 0.15, Ni 25, Mo 6	76-Percent reduction; start at 1900° F, finish at 1475° F	Rockwell C-27 to C-31
Overaged 16-25-6	As above	Blanks cut from hot-rolled bar. 2150° F, 5 min air-cooled, 1700° F, 24 hr in argon	Rockwell B-86 to B-92

TABLE II. - TENSILE PROPERTIES<sup>a</sup> OF TEST MATERIALS

Material	Unnotched bars						Notched bars					
	Room temperature			1300° F			Room temperature		1300° F			
	0.2-Percent offset yield strength, ksi	Ultimate strength, ksi	Ductility Percent reduction in area	Ductility $\ln \frac{A_i}{A_f}$	0.2-Percent offset yield strength, ksi	Ultimate strength, ksi	Percent reduction in area	Ductility $\ln \frac{A_i}{A_f}$	Ultimate strength, ksi	Percent reduction in area		
A-286	99.7	143	32.7	0.40	880	97.2	13.2	0.14	148	13.9	104	7.8
Discaloy	82.4	135	41.2	.53	b73	88.2	28.6	.34	145	14.5	88.2	11.0
Hot-cold worked 16-25-6	117.0	135	37.0	.46	c63	74.5	40.8	.52	154	11.8	85.4	11.2
Overaged 16-25-6	42.0	104	22.8	.26	---	60.6	24.4	.28	99.6	9.8	69.7	17.2

<sup>a</sup>All data are NASA and are average of two tests except as noted by b and c.

<sup>b</sup>Ward F. Simons and Howard C. Cross: The Elevated Temperature Properties of Selected Super-Strength Alloys. ASTM STP No. 160, 1954.

<sup>c</sup>Martin Fleischmann: The Development of the 16-25-6 Alloy for Gas Turbine and Turbo-Supercharger Applications. Timken Roller Bearing Co.

TABLE III. - COMPARISON OF CALCULATED WITH MEASURED TOTAL  
STRAIN RANGES AT DISK RIM

Material	Geometry	$\epsilon_{o,max}$ , in./in. (eq. (4))	Measured $\Delta r$ , in.	$\epsilon_T$ , in./in. (eq. (5))	$\left(\frac{\epsilon_{o,max} - \epsilon_T}{\epsilon_{o,max}}\right) 100$ , percent	$T_{max}$ , °F
Hot-cold worked 16-25-6	Unnotched	0.0079	0.0079	0.0079	0	1300
Hot-cold worked 16-25-6	Unnotched	.0066	.0062	.0068	-3	1100
Hot-cold worked 16-25-6	Notched	.0066	.0064	.0067	-2	1100
A-286	Notched	.0066	.0062	.0068	-3	1100
Discaloy	Notched	.0066	.0065	.0068	0	1100



TABLE V. - SUMMARY OF ROOM-TEMPERATURE MECHANICAL-FATIGUE DATA

(a) Notched rectangular bars

Material	Compression cycled										Tension cycled					
	$\epsilon_T = 0.0075$					$\epsilon_T = 0.0043$					$\epsilon_T = 0.0043$					
	$N_f$ , cycles	$S_M$ , ksi	$S_T$ , ksi	$\frac{N_{SM}}{N_f}$ , percent	$\frac{N_{ST}}{N_f}$ , percent	$N_f$ , cycles	$S_M$ , ksi	$S_T$ , ksi	$\frac{N_{SM}}{N_f}$ , percent	$\frac{N_{ST}}{N_f}$ , percent	$N_f$ , cycles	$S_M$ , ksi	$S_T$ , ksi	$\frac{N_{SM}}{N_f}$ , percent	$\frac{N_{ST}}{N_f}$ , percent	
A-286	1329	-15.3	198	61	88	188,780	-50.3	121	87	>93	3417	40.3	128	--	--	
Discaloy	1704	-18.7	193	69	94	50,625 62,475	-31.2 -31.4	124 121	>93 88	90 50	5422	29.4	122	94	72	
Hot-cold worked 16-25-6	903	-20.3	201	68	88	192,800	-51.7	124	86	95	2737	45.9	125	81	100	
Overaged 16-25-6	376 450	-1.0 -8.3	122 122	>69	>69	6,457 8,613	-6.8 -7.8	97 96	>66 80	>93	5986 6685	1.6 1.0	92 90	60 52	80 55	

TABLE V. - Concluded. SUMMARY OF ROOM-TEMPERATURE MECHANICAL-FATIGUE DATA

(b) Unnotched bars

Material	Rectangular section, $\epsilon_T = 0.0075$						Cylindrical section, $\epsilon_T = 0.0070$											
	Compression cycled						Compression cycled						Tension cycled					
	$N_f$ , cycles	$S_M$ , ksi	$S_T$ , ksi	$\frac{N_{S_M}}{N_f}$ , percent	$\frac{N_{S_T}}{N_f}$ , percent		$N_f$ , cycles	$S_M$ , ksi	$S_T$ , ksi	$\frac{N_{S_M}}{N_f}$ , percent	$\frac{N_{S_T}}{N_f}$ , percent		$N_f$ , cycles	$S_M$ , ksi	$S_T$ , ksi	$\frac{N_{S_M}}{N_f}$ , percent	$\frac{N_{S_T}}{N_f}$ , percent	
A-286	9,366	-10.6	157	70	53		12,250	-15.8	158	96	87		7,031	20.0	151	60	66	
	10,373	-10.6	157	52	~30													
Disalloy	9,622	-18.2	157	90	96		25,856	-15.2	144	79	78		14,285	11.9	139	56	86	
	12,531	-18.2	157	95	69													
Hot-cold worked 16-25-6	10,824	-17.0	166	86	88		38,225	-30.3	152	93	86		18,775	40.0	125	80	~100	
	11,551	-20.4	161	>96	>96													
Overaged 16-25-6	7,285	-4.3	94	>95	>95		12,410	-4.4	88	>87	>87		6,548	4.5	90	>93	>97	
	7,673	-5.3	96	>96	>96		11,279	-4.4	92	99	99		14,231	-0.6	91	>97	>97	

TABLE VI. - CRACK-SIZE MEASUREMENTS IN NOTCHED BARS  
 SUBJECTED TO MECHANICAL FATIGUE  
 AT ROOM TEMPERATURE

$\epsilon_T = 0.0043$ ; compression cycled						
Material	$N_f$ , cycles	N at inspection, cycles	$N/N_f$ , percent	$S_M$ , ksi	$S_T$ , ksi	Crack area (percent original test- section area)
Discalloy	50,625	38,875	77	-31.2	124	33
Hot-cold worked 16-25-6	192,800	37,914 56,126	20 29	-51.7 -51.7	124 124	17 37

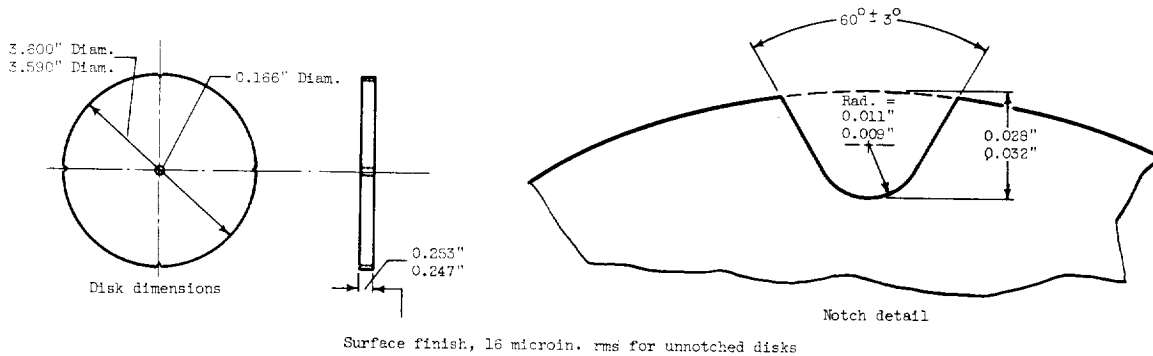
TABLE VII. - NOTCHED-DISK THERMAL-FATIGUE CALCULATED AND MEASURED  
 INCIPIENT FAILURE COMPARISONS - NO HOLD TIME

Material	Maximum cycle temperature, °F	Nominal strain range, in./in.	Predicted life, based on room-temperature tensile ductility, $N_{p,min}$ cycles	Predicted life, based on 1300° F tensile ductility, $N_{p,max}$ cycles	Actual crack area at $N_{p,min}$ sq mils	Actual crack area at $N_{p,max}$ sq mils
Discaloy	1300	0.0074	110	45	2350	<250
	1300	.0066	146	60	3400	<250
	1300	.0054	252	104	5250	650
	1300	.0043	487	200	6100	1350
	1100	.0066	148	61	2400	850
	1100	.0054	254	105	1630	350
	1100	.0043	495	204	500	<250
	A-286	1300	0.0074	66	8	650
1300		.0066	88	11	800	<250
1300		.0054	155	19	1875	<250
1300		.0043	310	38	1600	<250
1100		.0066	90	11	550	<250
1100		.0054	158	19	<250	<250
1100		.0043	320	39	400	<250
Hot-cold worked 16-25-6		1300	0.0079	73	97	>>6000
	1300	.0066	116	153	>>6000	>>6000
	1300	.0054	202	268	>>6000	>>6000
	1300	.0043	401	532	>>6000	>>6000
	1100	.0066	120	159	2400	5000
	1100	.0054	212	281	500	1750
	1100	.0043	428	568	1100	2650
	Overaged 16-25-6	1300	0.0079	18	21	<250
1300		.0066	27	31	<250	<250
1300		.0054	43	50	<250	<250
1300		.0043	74	86	<250	<250
1100		.0066	27	31	<250	<250
1100		.0054	43	50	<250	<250
1100		.0043	73	85	<250	<250

TABLE VIII. - ACTUAL AND CALCULATED MECHANICAL-FATIGUE LIVES FOR UNNOTCHED BARS AT ROOM TEMPERATURE

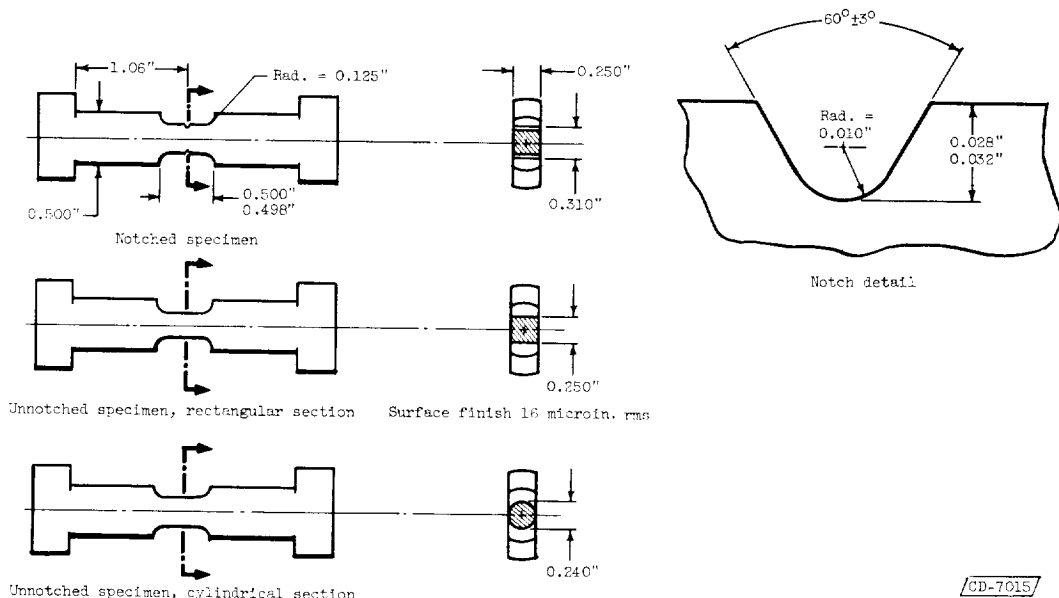
Material	Specimen geometry	Nominal strain range, $\epsilon_T$ , in./in.	Direction of initial loading	Measured life, $N_f$ , cycles	Predicted life, based on plastic strain computed from measured stress range, $N_{p,1}$ , cycles	$N_{p,1}/N_f$	Predicted life, based on plastic strain computed from twice yield stress, $N_{p,2}$ , cycles	$N_{p,2}/N_f$
A-286	Rectangular	0.0075	Compression	9,366	8,300	0.887	68,600	7.33
	Rectangular	.0075	Compression	10,373	8,300	.800	68,600	6.61
	Cylindrical	.0070	Compression	12,250	14,480	1.18	576,000	47.0
	Cylindrical	.0070	Tension	7,031	11,100	1.42	576,000	82.0
Discaloy	Rectangular	0.0075	Compression	9,622	18,060	1.875	24,400	2.54
	Rectangular	.0075	Compression	12,531	18,060	1.44	24,400	2.54
	Cylindrical	.0070	Compression	25,856	18,850	.73	49,000	1.90
	Cylindrical	.0070	Tension	14,285	15,830	1.11	49,000	3.43
Hot-cold worked 16-25-6	Rectangular	0.0075	Compression	10,824	20,320	1.875	$\infty$	$\infty$
	Rectangular	.0075	Compression	11,551	16,500	1.428	$\infty$	$\infty$
	Cylindrical	.0070	Compression	38,225	20,410	.533	$\infty$	$\infty$
	Cylindrical	.0070	Tension	18,775	8,030	.428	$\infty$	$\infty$
Overaged 16-25-6	Rectangular	0.0075	Compression	7,285	970	0.133	827	0.115
	Rectangular	.0075	Compression	7,673	1,010	.132	827	.108
	Cylindrical	.0070	Compression	12,410	1,120	.090	1,045	.084
	Cylindrical	.0070	Compression	11,279	1,210	.107	1,045	.093
	Cylindrical	.0070	Tension	6,548	1,170	.179	1,045	.16
Cylindrical	.0070	Tension	14,231	1,190	.084	1,045	.073	

E-825



(a) Thermal fatigue.

CY-6



(b) Mechanical fatigue.

Figure 1. - Fatigue specimen configurations.

CD-7015

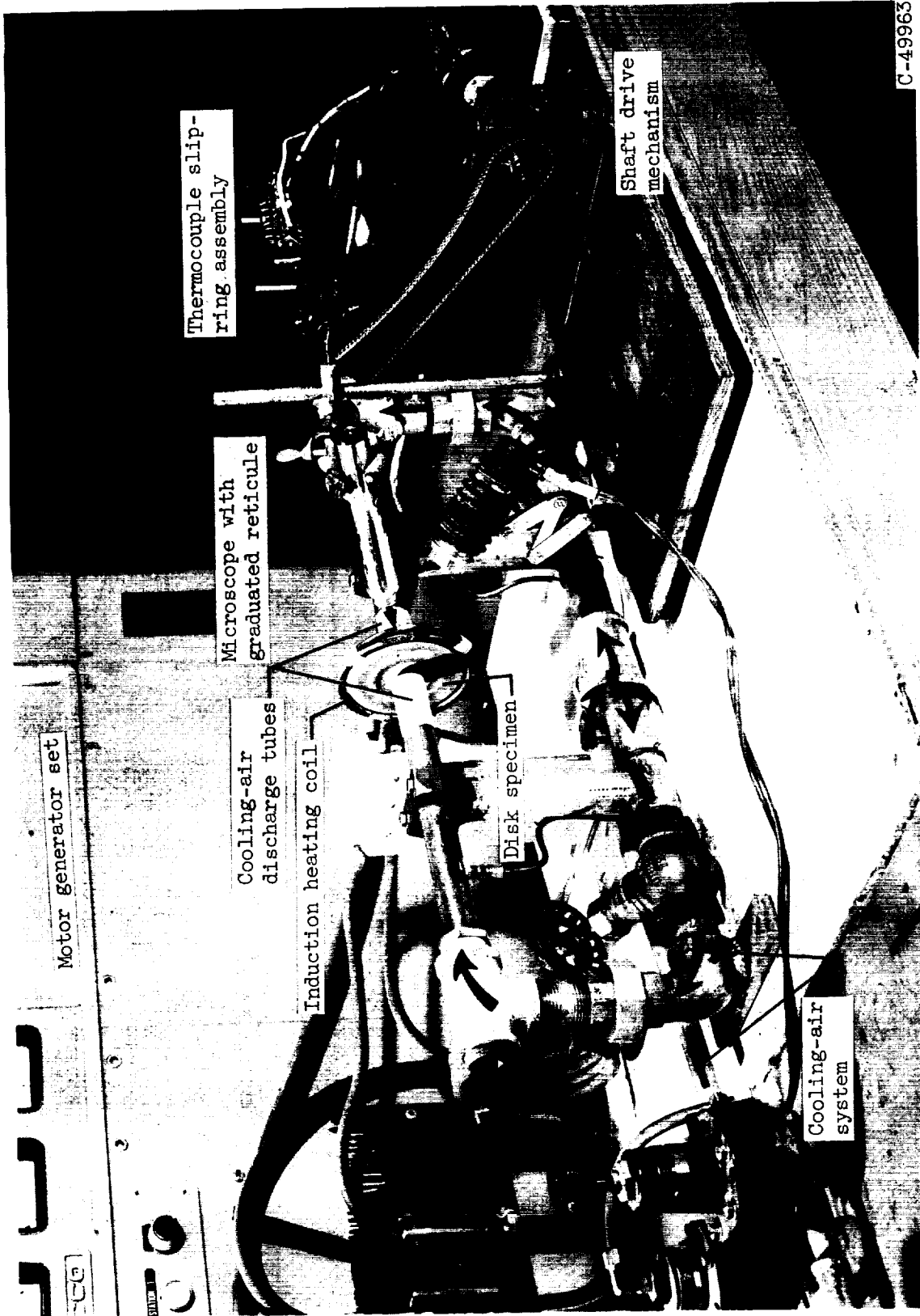
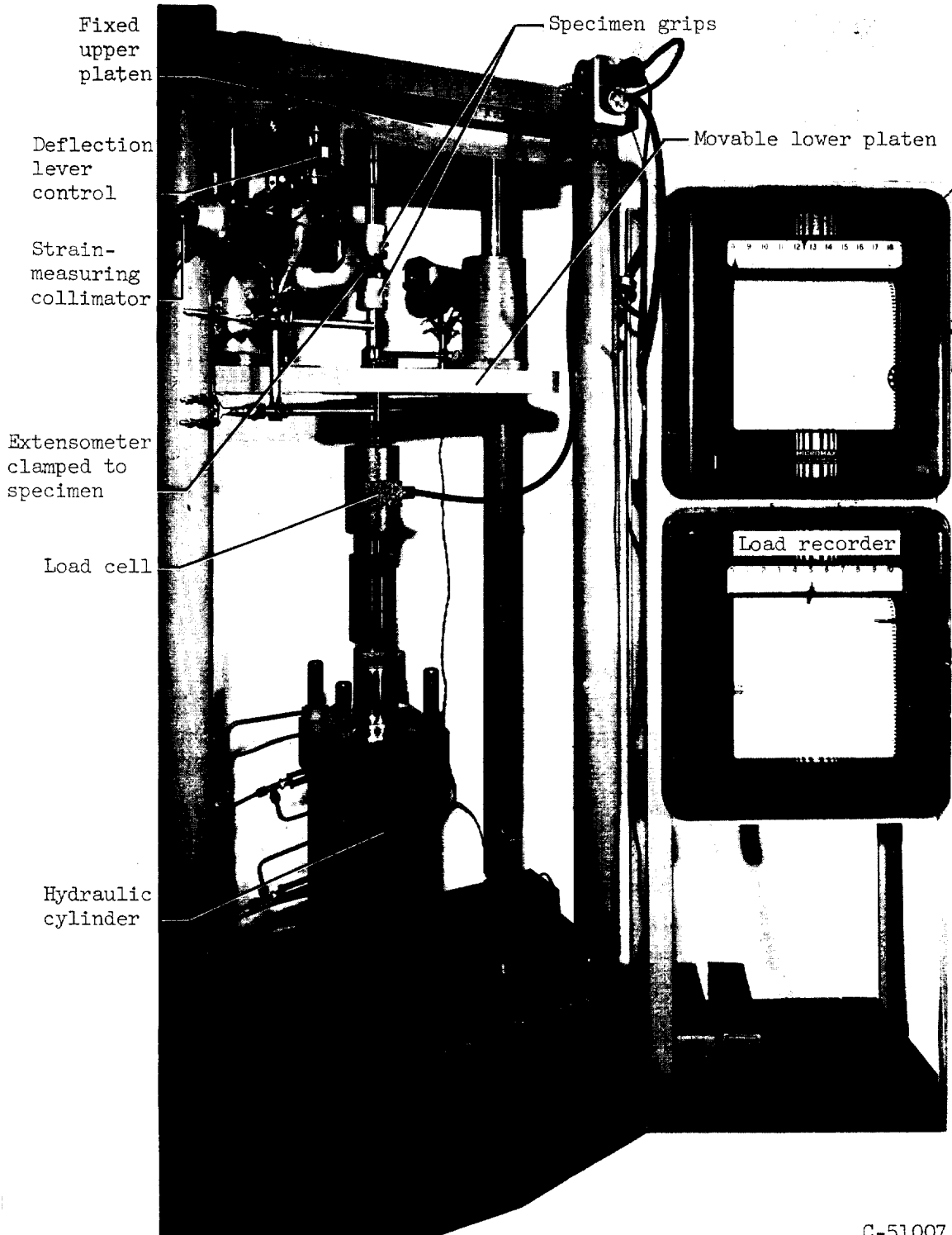


Figure 2. - Thermal-fatigue test rig.

E-825

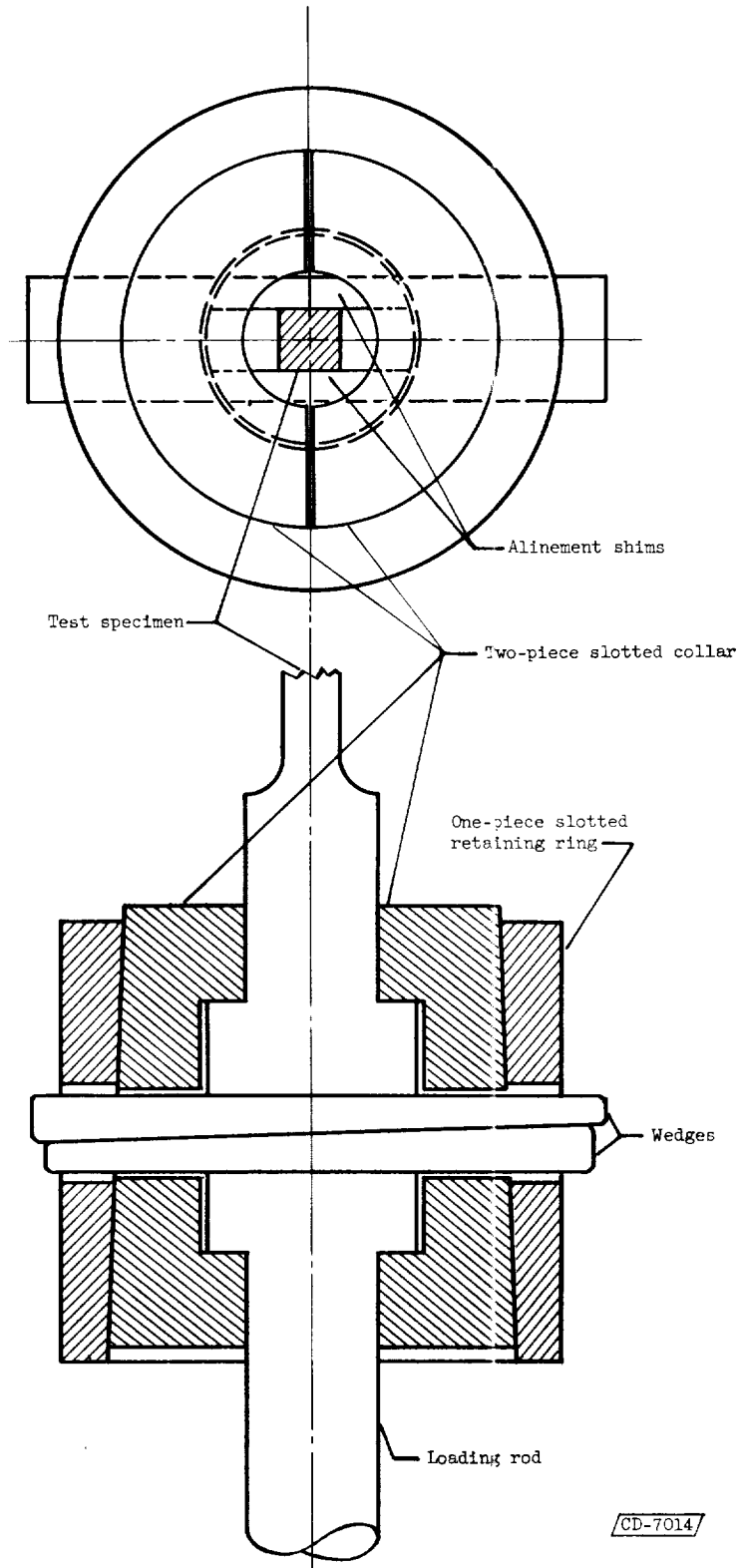
CY-6 back



C-51007

(a) Overall assembly.

Figure 3. - Mechanical low-cycle fatigue apparatus.



(b) Mechanical-fatigue specimen grip.

Figure 3. - Concluded. Mechanical low-cycle fatigue apparatus.

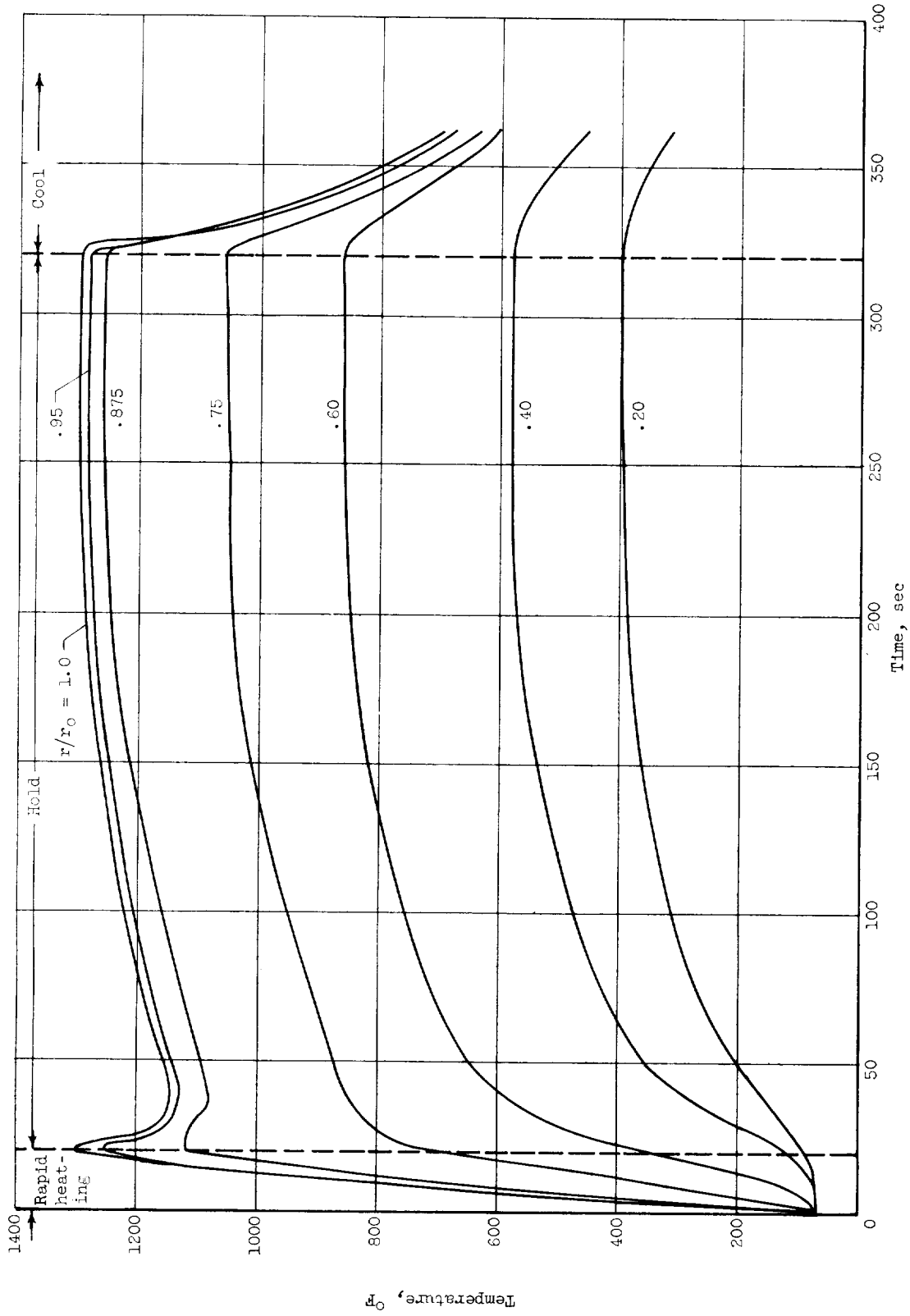
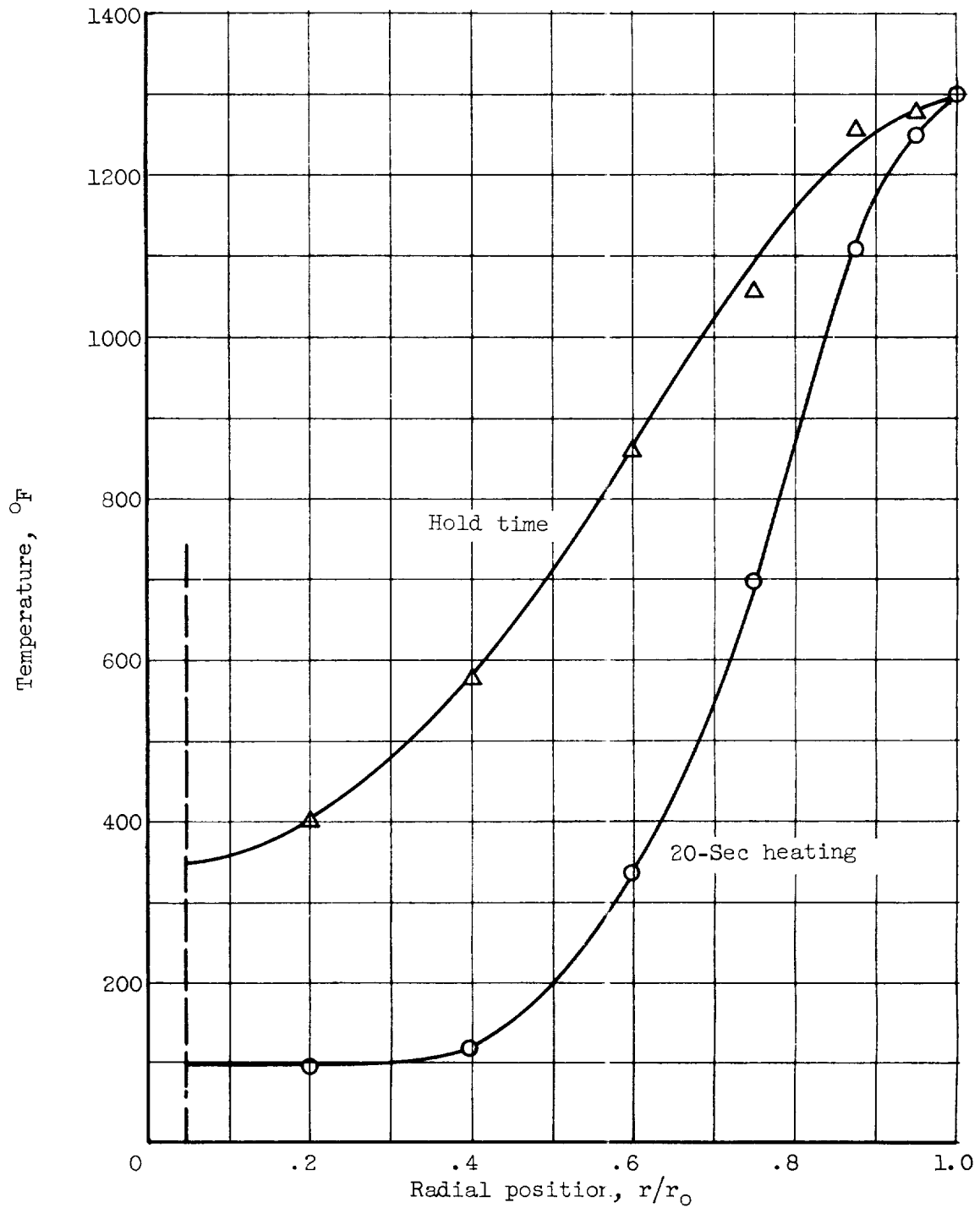


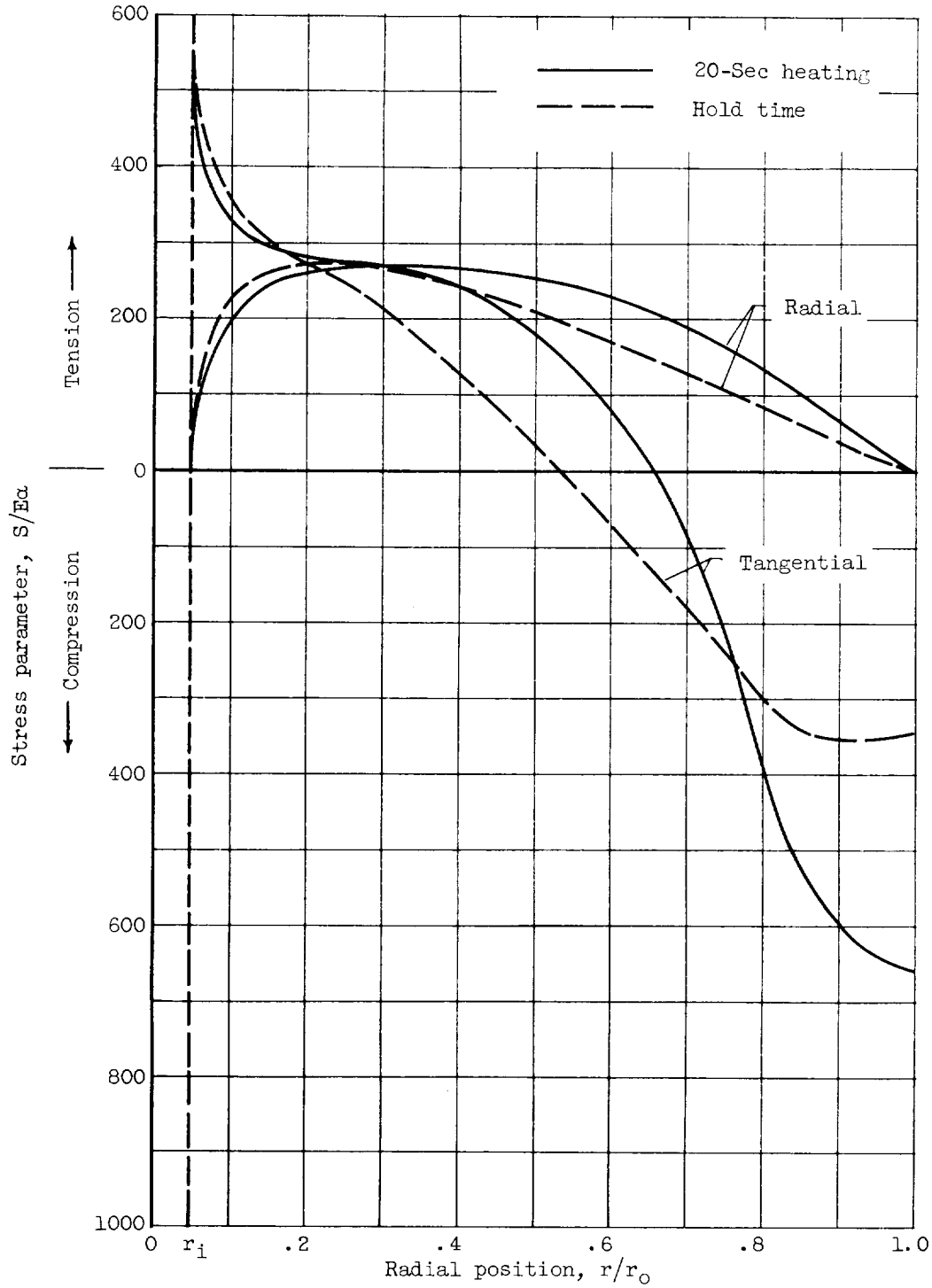
Figure 4. - Variation of disk temperature during fast heat, hold, and start of cooling period.



(a) Temperature distribution.

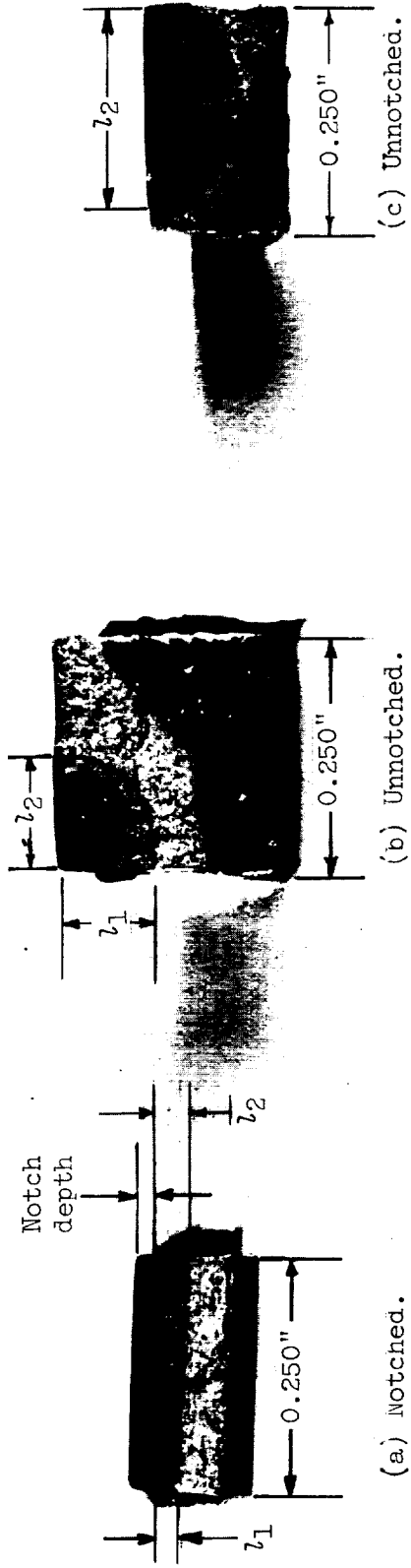
Figure 5. - Temperature and stress distributions in disk specimen at end of 20-second heat to 1300° F and at end of 5-minute hold period at 1300° F.

E-825



(b) Elastically computed radial and tangential stresses.

Figure 5. - Concluded. Temperature and stress distributions in disk specimen at end of 20-second heat to 1300° F and at end of 5-minute hold period at 1300° F.



C-50884

Figure 6. - Disk thermal-fatigue fracture surfaces.

E-825

CY-7

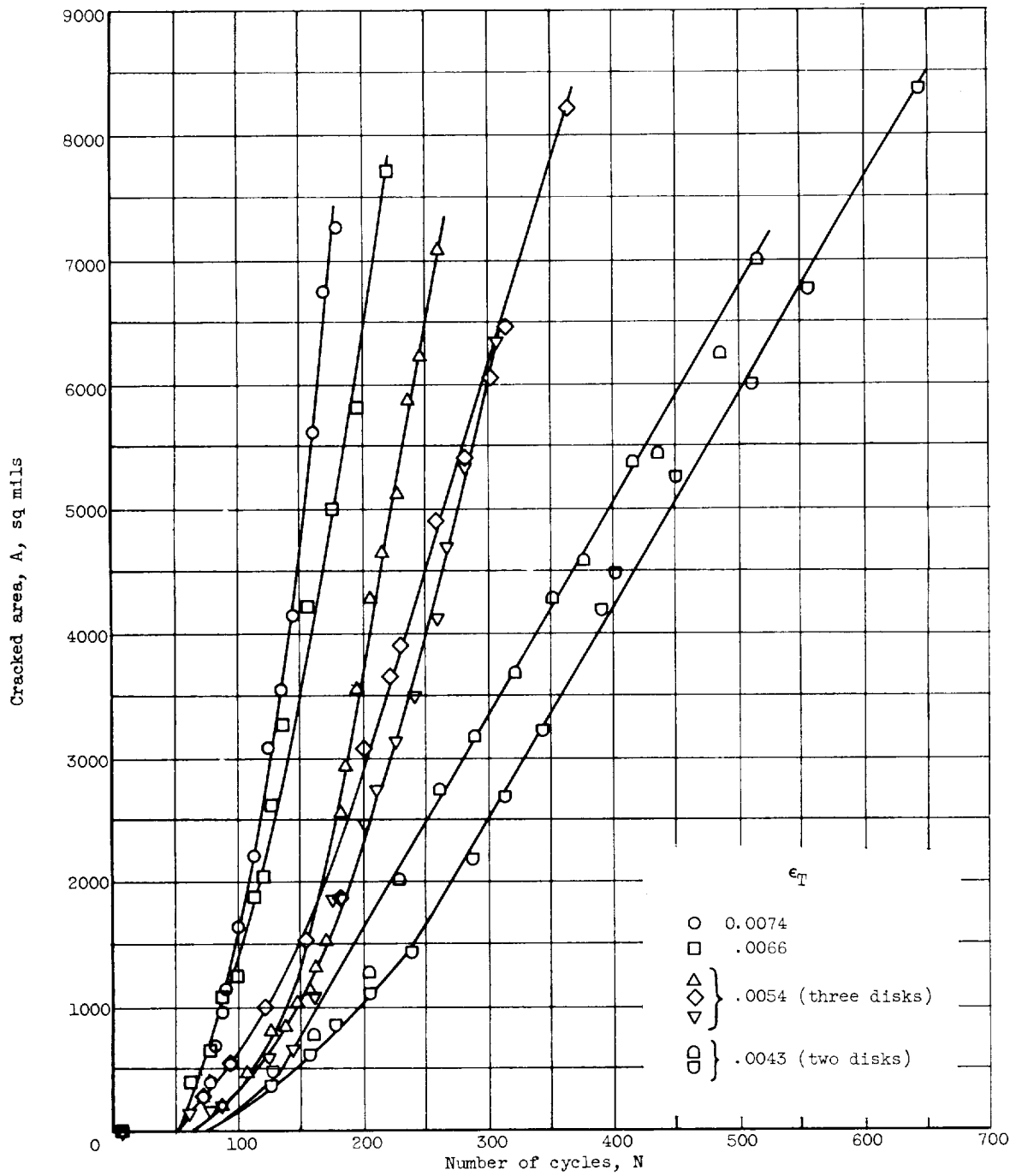
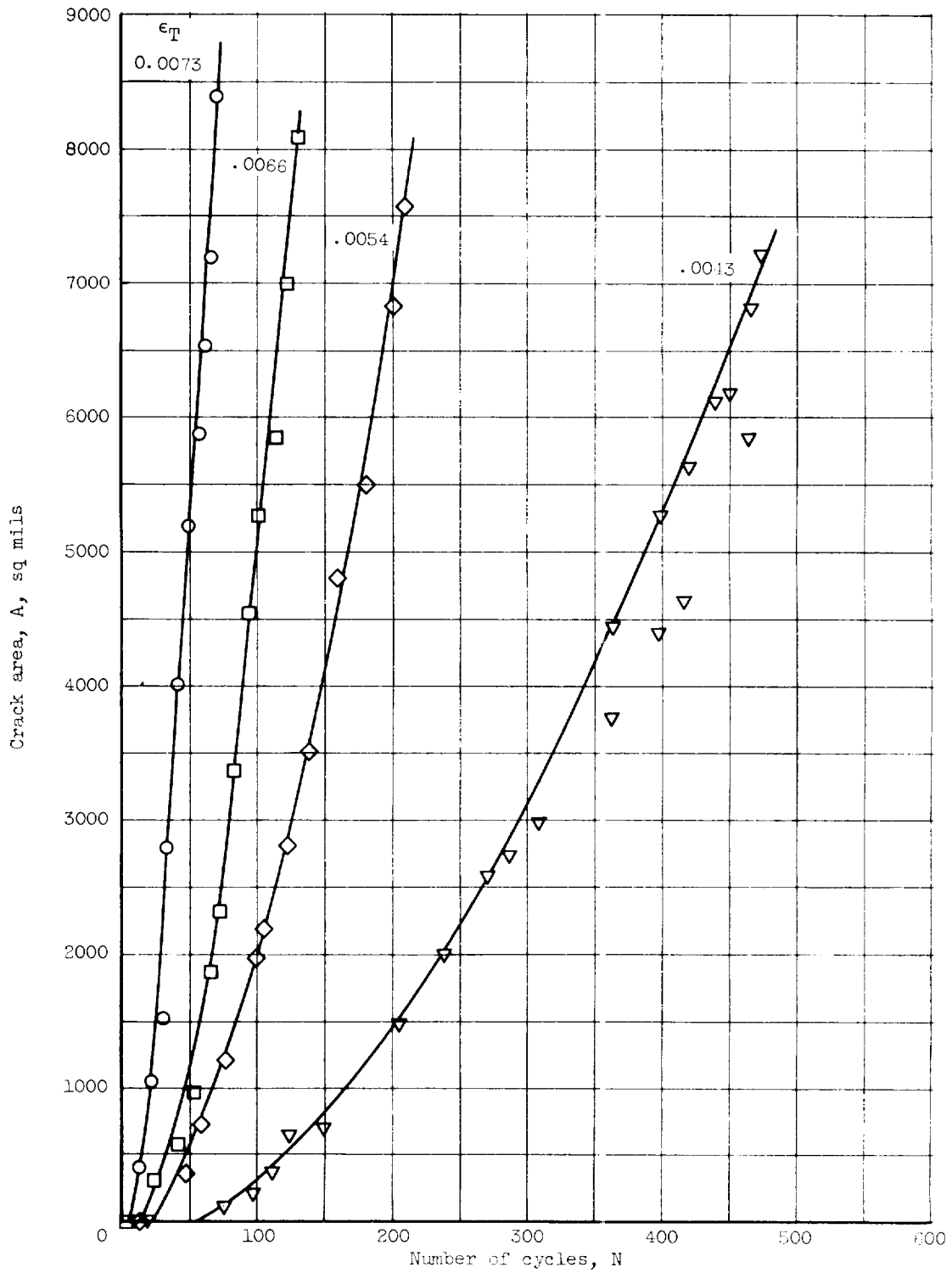


Figure 7. - Crack-growth data for notched Discalloy disks.



(b)  $T_{max} = 1300^{\circ} F$ ; 5-minute hold at  $T_{max}$ .

Figure 7. - Continued. Crack-growth data for notched Discaloy disks.

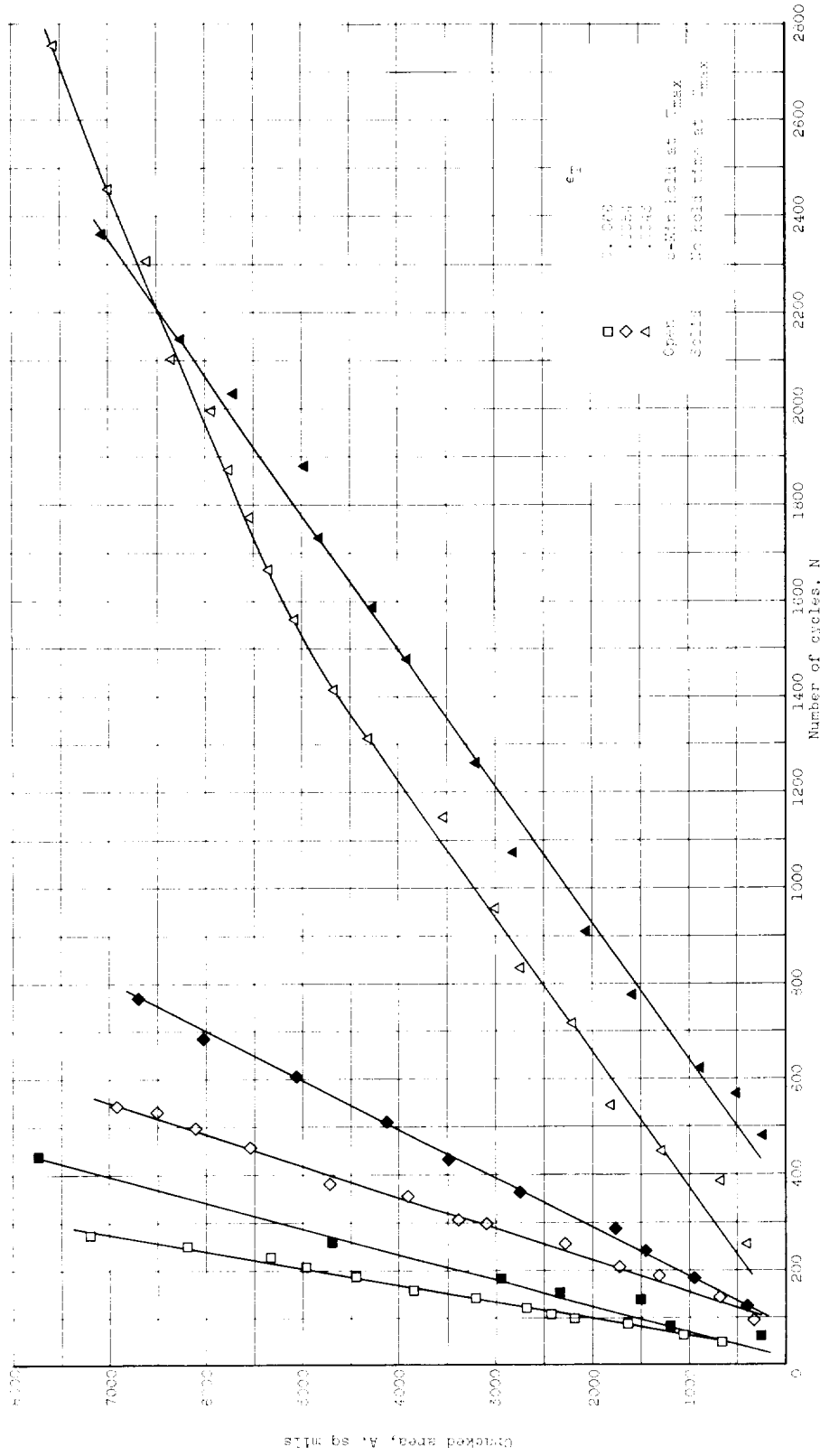


Figure 7. - Concluded. Crack-growth data for notched Discaloy disks.

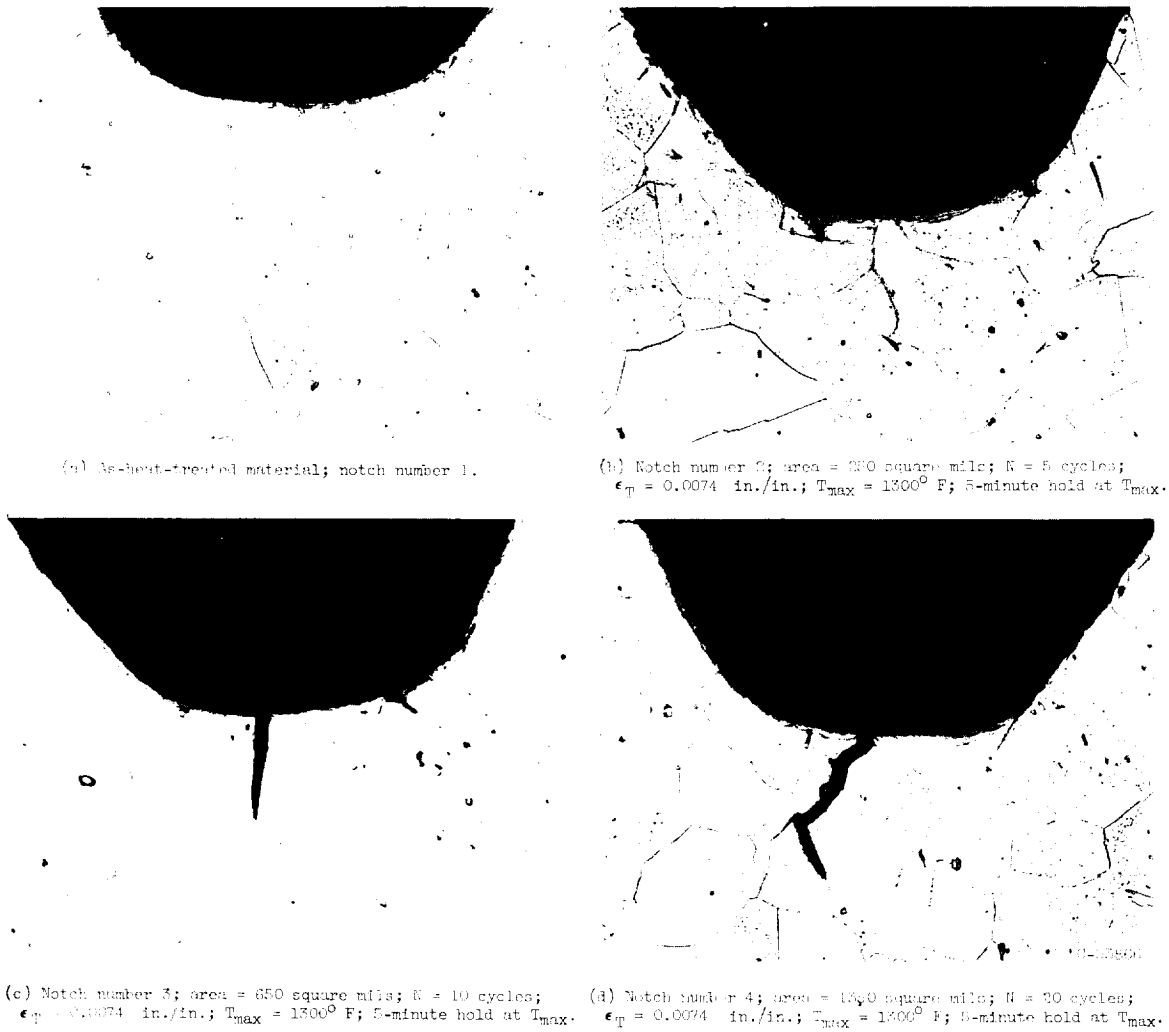
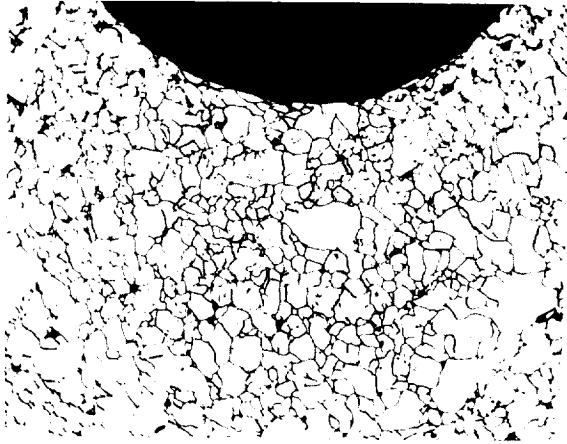


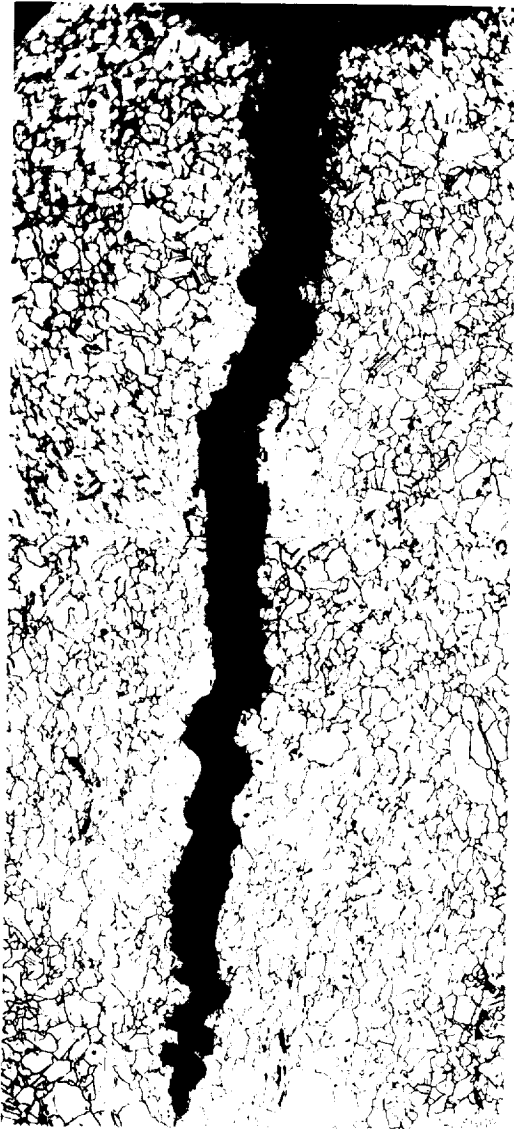
Figure 8. - Effect of thermal-fatigue conditions on microstructure of A-36. Etchant: 50 percent  $H_2O$ , 40 percent  $HCl$ , 10 percent  $HNO_3$ . X250. Picture reduced 48 percent in reproduction.



Figure 9. - Effect of thermal-fatigue conditions on microstructure of Inconel. Etchant: 50 percent  $H_2O$ , 40 percent HCl, 10 percent  $HNO_3$ . Picture reduced 40 percent in reproduction.

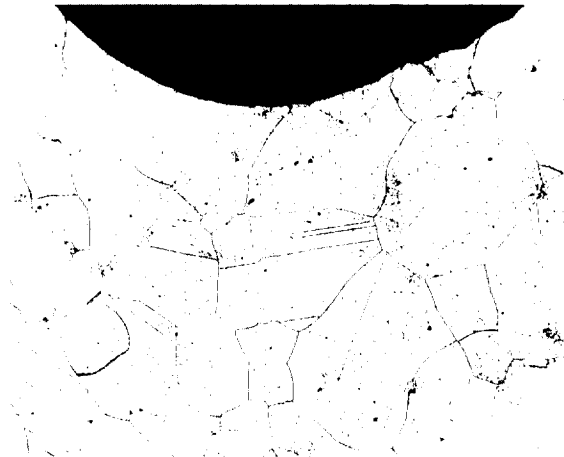


(a) Hot-cold worked 10-15-0; as heat-treated.



(b) Hot-cold worked (as in (a)) after 21,000 cycles;  $\epsilon_{max} = 0.0075$  (one per cent  $\epsilon_{max}$  at 1800°C) (reference note 1).

Figure 1. - Effect of thermal-fatigue conditions on microstructure of hot-cold worked and aged 10-15-0. (Sheet: 50 percent Rp, 10 percent Rp, 10 percent Rp, and 20% X200. Magnification 10 percent in reproduction.)



(c) Overaged 16-25-6; no heat-treatment.



(d) Overaged 16-25-6 after 157 cycles;  $\epsilon_{max} = 0.0079$   
Inch per inch;  $T_{avg} = 1300^{\circ}F$ ; no hold time.

Figure 10. - Continued. Effect of Elong-to-Fatigue conditions on microstructures of hot-cold worked and overaged 16-25-6. Etchant: 50 percent  $H_2O$ , 40 percent  $HCl$ , 10 percent  $HNO_3$ . X150. Picture reduced 42 percent in reproduction.

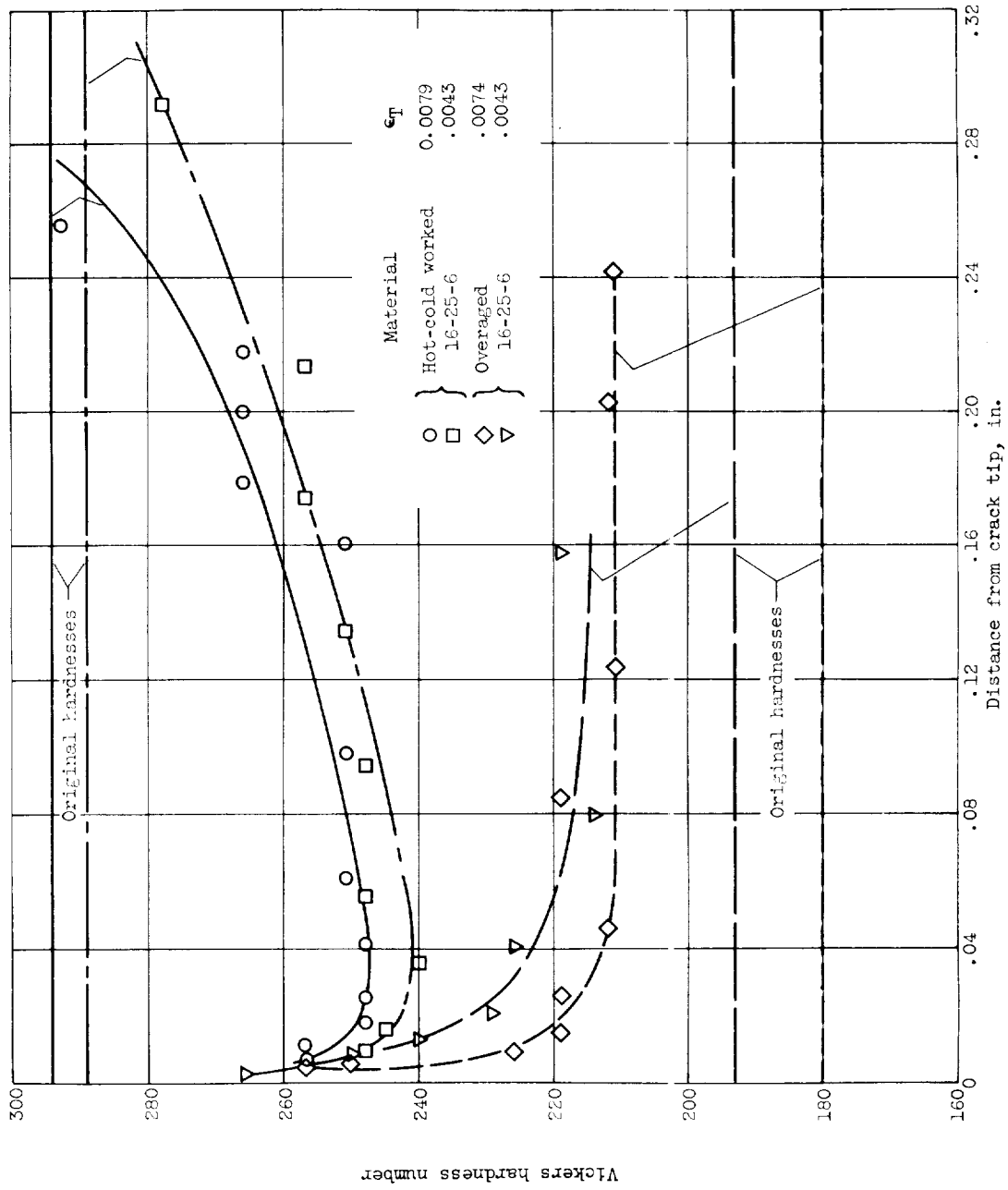


Figure 11. - Microhardness surveys on notched hot-cold worked 16-25-6 and overaged 16-25-6 disks following thermal-fatigue cycling.  $T_{max} = 1300^{\circ}$ ; 5-minute hold at  $T_{max}$ .

R-825

CY-8

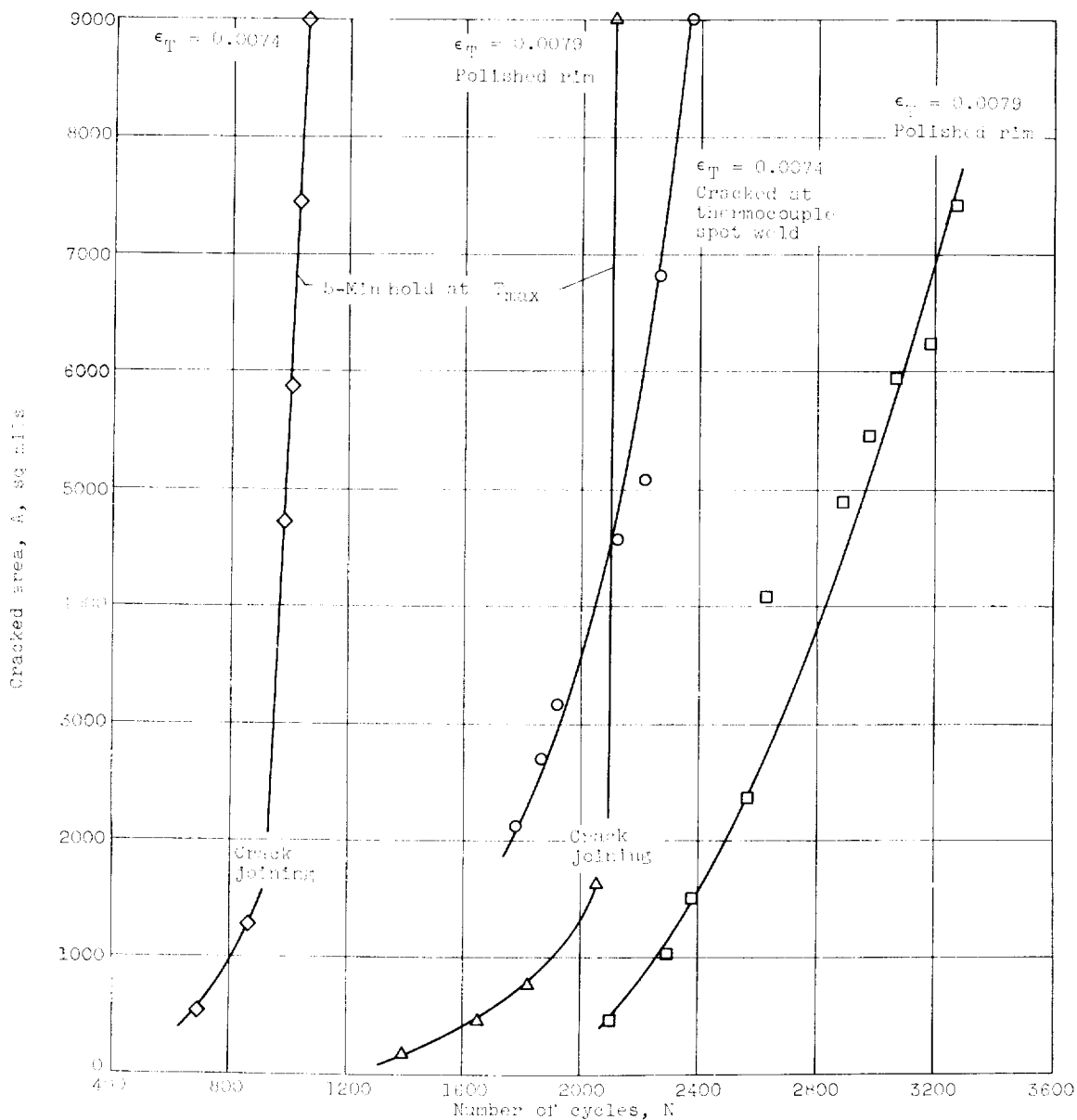


Figure 12. - Crack-growth data for unnotched Discalloy disks.  $T_{max} = 1300^{\circ} F.$



